Calhoun
Institutional Archive of the Naval Postgraduate School

Calhoun: The NPS Institutional Archive

Theses and Dissertations | Thesis Collection

1964

The distribution of tropospheric velocity divergence with respect to pressure systems

Alden, Robert F.

Monterey, California. Naval Postgraduate School

http://hdl.handle.net/10945/12025

DUDLEY KNOX LIBRARY

http://www.nps.edu/library

Calhoun is a project of the Dudley Knox Library at NPS, furthering the precepts and goals of open government and government transparency. All information contained herein has been approved for release by the NPS Public Affairs Officer.

Dudley Knox Library / Naval Postgraduate School
411 Dyer Road / 1 University Circle
Monterey, California USA 93943

NPS ARCHIVE
1964
ALDEN, R.

THE DISTRIBUTION OF TROPOSPHERIC VELOCITY DIVERGENCE WITH RESPECT TO PRESSURE SYSTEMS

ROBERT F. ALDEN
GLEN C. ROSENBERGER

DUDLEY KNOX LIBRARY
NAVAL POSTGRADUATE SCHOOL
MONTEREY CA 93943-5101

LIBRARY
U.S. NAVAL POSTGRADUATE SCHOOL
MONTEREY, CALIFORNIA

THE DISTRIBUTION OF TROPOSPHERIC VELOCITY DIVERGENCE WITH RESPECT TO PRESSURE SYSTEMS

* * * * *

Robert F. Alden

and

Glenn C. Rosenberger

THE DISTRIBUTION OF TROPOSPHERIC VELOCITY DIVERGENCE WITH RESPECT TO PRESSURE SYSTEMS

BY

Robert F. Alden

Lieutenant, United States Navy

and

Glenn C. Rosenberger

Lieutenant, United States Navy

Submitted in partial fulfillment of
the requirements for the degree of

MASTER OF SCIENCE
IN
METEOROLOGY

United States Naval Postgraduate School
Monterey, California

1 9 6 4

NPS Archive
1964
Alden, R.

Thesis
A34

LIBRARY
U.S. NAVAL POSTGRADUATE SCHOOL
MONTEREY, CALIFORNIA

THE DISTRIBUTION OF TROPOSPHERIC VELOCITY DIVERGENCE WITH RESPECT TO PRESSURE SYSTEMS

by

Robert F. Alden

and

Glenn C. Rosenberger

This work is accepted as fulfilling
the thesis requirements for the degree of
MASTER OF SCIENCE
IN
METEOROLOGY
from the
United States Naval Postgraduate School

ABSTRACT

With the aid of an electronic computer, velocity divergence, vertical velocity, and thermal advection computations are performed at the standard pressure levels. These parameters are then related to tropospheric pressure systems, classified according to subsequent development or non-development. Typical plan view and cross section patterns are presented.

The writers wish to express their appreciation to Professor George J. Haltiner of the U. S. Naval Postgraduate School for his guidance and assistance in this study. Appreciation is also expressed to the personnel of the U. S. Navy Fleet Numerical Weather Facility for their cooperation during the preparation of this paper. We are especially indebted to CDR. L. C. Clarke and LCDR M. Jane Seljos for their aid and programming assistance.

TABLE OF CONTENTS

Section	Title	Page
1.	Introduction	1
2.	Background	2
3.	Procedures	6
4.	Case studies	8
5.	Thermal advection	17
6.	Summary	19
7.	Illustrations	21
8.	Bibliography	59

TABLE OF SYMBOLS

R -- the universal gas constant

D -- the difference between the height of the pressure surface and the atmospheric value: $D = Z - Z_p$

T -- the atmospheric temperature

p -- the atmospheric pressure

f -- the coriolis parameter, $2\Omega \sin\phi$, where ϕ is the geographic latitude

$\bar{f}$ -- the coriolis parameter where $\phi = 45N$

m -- the map scale factor: $m(\phi) = \frac{1 + \sin 60}{1 + \sin \phi}$

g -- the acceleration of gravity

d -- grid distance, 381 km, true at 60N

ω -- the vertical velocity of air in pressure coordinates

σ -- the static stability parameter: $\sigma = -\frac{T}{\theta}\frac{\partial \theta}{\partial p}$

ζ -- the relative vorticity: $\zeta = \frac{\partial v}{\partial x} - \frac{\partial u}{\partial y}$

J -- the horizontal Jacobian operator: $J(A,B) = \frac{\partial A}{\partial x}\frac{\partial B}{\partial y} - \frac{\partial A}{\partial y}\frac{\partial B}{\partial x}$

∇^2 -- the horizontal Laplacian operator on a constant-pressure surface

∇ -- the del operator on a constant-pressure surface

V_ψ -- the non-divergent portion of the wind

V_χ -- the divergent portion of the wind

$\mathcal{J}$ -- the finite-difference Jacobian:

$$\mathcal{J}(A,B) = \left[(A_{i+1,j} - A_{i-1,j})(B_{i,j+1} - B_{i,j-1})\right] - \left[(A_{i,j+1} - A_{i,j-1})(B_{i+1,j} - B_{i-1,j})\right]$$

1. Introduction.

The importance of vertical motion and divergence as related to the development and the dissipation of tropospheric pressure systems has long been of interest to the synoptic meteorologist.

It is the purpose of this research to investigate the tropospheric distribution of vertical motion, velocity divergence, and thermal advection with the divergent and non-divergent winds. Previous writers on these subjects have usually limited their investigations to a small data sample. Since numerical techniques of analysis have been utilized in this study, numerous synoptic situations from a relatively large data sample have been considered.

2. Background.

Vertical velocity, ω , was computed by the diagnostic equation

$$\nabla^2(\sigma\omega) + \frac{p f \eta}{R}\frac{\partial^2\omega}{\partial p^2} = \nabla^2\left[\frac{g}{f}J(D,T)\right] - J(T,\eta) - J\left(D, \frac{g}{f}\nabla^2 T\right) \qquad (1)$$

developed by Haltiner, Clarke, and Lawniczak [3]. Here D is the difference between the height of the pressure surface and the standard atmospheric value, $\eta = f + f$, and $\omega = \frac{dp}{dt}$.

The following boundary conditions were imposed in the calculation of ω values. For the upper boundary condition, $\omega = 0$ at 100 mb. At the lower boundary terrain-forced vertical motion and frictionally-induced vertical motion are combined to give net vertical motion which is applied at the surface of the earth. A detailed description of the development and of the boundary conditions can be found in [3] . Omega values were computed by the U. S. Navy Fleet Numerical Weather Facility, Monterey, California, as a part of normal operations.

Values of velocity divergence were calculated using the continuity equation in pressure coordinates

$$\nabla_p \cdot V = -\frac{\partial\omega}{\partial p} \qquad (2)$$

as the working equation. The right side of (2) was approximated by a finite-difference expression to obtain divergence at the 1000, 850, 700, 500, and 300-mb pressure surfaces.

Divergence at 1000 mb was computed by approximating the derivative with the forward-difference formula

$$-\frac{\partial \omega}{\partial p} = -\left[\frac{[(p_0-p_1)+(p_2-p_0)](\omega_1-\omega_0)}{(p_0-p_1)(p_2-p_0)}\right] - \left[\frac{(p_0-p_1)(\omega_2-\omega_0)}{(p_2-p_0)(p_2-p_1)}\right] \qquad (3)$$

Figure 1a depicts the division of the atmosphere for this computation. Where the terrain pressure was greater than 1000 mb, the terrain was used as the base level of the derivative. Where terrain pressure was less than 1000 mb, divergence was not computed. The derivative at the remaining levels was approximated by the central-difference formula

$$-\frac{\partial \omega}{\partial p} = \frac{(\omega_0-\omega_1)(p_2-p_1)}{(p_1-p_0)(p_2-p_0)} - \frac{(p_1-p_0)(\omega_2-\omega_1)}{(p_2-p_1)(p_2-p_0)} \qquad (4)$$

Figure 1b depicts the division of the atmosphere for these calculations. Prior to calculation of divergence at these levels, the terrain pressure was taken into account in the following manner: where the terrain pressure was less than the pressure at the computation level, p_1, divergence was not computed for that particular level; where terrain pressure was greater than the pressure at p_o, p_o was used as the base level of the derivative; where terrain pressure was greater than the pressure at p_1 and less than the pressure at p_o, the terrain level was used as the base level of the derivative. In the latter case if the interval p_o to p_1 was less than 25 mb, the latter was used for the interval.

The horizontal advection rate takes the form

$$-\mathbb{V}\cdot\nabla T \tag{5}$$

where $\mathbb{V}=\mathbb{V}_\chi$ and $\mathbb{V}=\mathbb{V}_\psi$ for the divergent and the non-divergent wind respectively. For convenience, the stream function, ψ, is redefined as follows, $\psi=\frac{g}{f}E$, where E has units of height. Consequently, thermal advection is given by the finite-difference expression

$$\frac{g}{f}\frac{m^2}{d^2}\,J(E,T) \tag{6}$$

The following finite-difference expression was used to compute thermal advection with the divergent wind where u_χ and v_χ are the components of the wind.

$$\frac{m}{2d}\left[u_\chi(T_{i+1}-T_{i-1})+v_\chi(T_{j+1}-T_{j-1})\right] \tag{7}$$

Advection was computed at the 1000, 850, 700, and 500-mb levels. The components of the divergent wind were computed by F. E. Lacey, Captain, United States Marine Corps, as a part of his thesis [4]. Fields of E were obtained by operating on D fields with the balance equation. Rates of thermal advection are expressed in degrees Centigrade per hour.

All computations were done on the Control Data Corporation Model 1604 computer using the U. S. Navy Fleet Numerical Weather Facility's square grid. This grid,

centered at the pole, consists of 3969 grid points with a grid point interval of 381 km at 60N. The period of investigation was 13 February to 1 April 1964.

3. Procedures

For the purpose of this study, segments of life cycles of tropospheric pressure systems will be classified as follows: moving-intensifying; moving-non-intensifying; and blocking. Systems were examined during that portion of their life cycle when they were located over a dense data area. Divergence computations over Mexico and similar sparce data areas were neglected since the magnitudes were sometimes unrealistic.

At the onset, a cross section type representation was thought to be the best way to depict the vertical distribution of divergence. However, this approach by itself did not always show the significant features of the divergence patterns. To remedy this, a combination of both cross section and plan views was used for data representation.

Figures 2 through 5 illustrate the variations in divergence patterns that can be obtained by changing the location of the cross section from line AA' to line EE'. This particular case represents the divergence distribution at 00Z 15 March through a 500-mb trough with the wind maximum east of the trough. The basic configurations are in agreement with the simplified trough model suggested by Stuart [5] and can be recognized in the actual case studies that follow.

In the cross sections, the heavy dashed (dotted) line is

the intersection of the pressure level and the trough (ridge) line. The slope of the trough and ridge lines are dependent on the orientation and location of the cross section. The distance between grid points on the cross sections is indicated as either 381 km or 538 km depending on the cross section orientation.

On the plan view presentation, solid lines represent divergence with a contour interval of 40×10^{-7} per second, positive areas being divergence and negative areas convergence. Dashed isobar (contour) lines for the surface (upper air) analysis are superimposed on the divergence fields.

The following are representative examples of the cases studied for each classification.

4. Case studies.

A. MIGRATORY LOW

Divergence and convergence patterns associated with moving-intensifying and moving-non-intensifying low pressure systems will be illustrated in this case. The patterns depicted are representative of those observed with ten other low pressure systems that traversed the United States during February and March 1964.

This case study, illustrated by figures 6a through 19b, covers the period from 00Z 17 March to 12Z 19 March 1964. A weak surface low, located over Michigan at 00Z 17 March, moved to the New Jersey coastal area by 00Z 18 March with little change in intensity. This portion of the system's life cycle was classified as moving-non-intensifying. From 12Z 18 March to 12Z 19 March the system deepened rapidly and moved to a position northeast of Nova Scotia. The central pressure of the low at 12Z 19 March was 972 mb. This portion of the system's life cycle was classified as moving-intensifying.

Figure 6a illustrates the surface pressure and 1000-mb divergence patterns for 00Z 17 March. Due to the terrain pressure being less than 1000 mb, divergence at 1000 mb was not computed for many areas of the United States. At 850 mb, figure 6b, the line of zero divergence was orientated north-south through the western sector of the low. Symmetrical centers of convergence and divergence of nearly

equal magnitude existed to the east and west of the low respectively. The convergence was associated with warm advection in the southerly flow, while the divergence was associated with cold advection in the northerly flow. By 500 mb, figure 7a, the pattern has reversed. Convergence (divergence) was observed west (east) of the trough. The small magnitudes of divergence, less than 50 x 10^{-7} per second, found at 500 mb appear to be characteristic of the moving-non-intensifying system. Typical upper tropospheric divergence patterns were clearly evident at the 300-mb level, figure 7b. Cross sections of vertical velocity and divergence are illustrated in figure 15. Small magnitude centers (less than 25 x 10^{-4} mb per second) of upward motion to the east and downward motion to the west of the trough were observed. The line of zero vertical velocity was nearly coincident with the trough line. In the divergence cross section a mid-tropospheric column of convergence, or the convergence enclosed by the -20 x 10^{-7} per second iso-line, was evident. This pattern has been described by Cressman [1]. However, significant deepening or intensification was not observed during this portion of the system's life cycle.

Figures 8 and 16a depict the divergence patterns for 12Z 17 March. At 850 mb little change in the magnitude or orientation of the patterns from those of 00Z 17 March was observed. Values at the 500-mb level were small. The

cross section was oriented east-west to the south of the 500-mb low center. The low level convergence observed to the west of the trough line was associated with another weak surface trough in that area.

At 00Z 18 March, figures 9, 16b and 17, a complex pattern of convergence and divergence was observed. This was due to the formation of a new surface low over New Jersey. Dual patterns of convergence and divergence were observed at 850 mb. Small magnitude centers were associated with the old 850-mb trough in Ohio, while the stronger centers were observed with the trough off of the New Jersey coast. A similar dual pattern was observed at 500 mb. The magnitudes of divergence at this level are greater than they were on 17 March. Figure 17 depicts the cross sections of vertical velocity and divergence associated with the new low. The magnitudes of vertical velocity were increased although the orientation of the patterns was the same as that on 17 March. Symmetrical patterns of divergence and convergence, similar to those suggested by Fleagle [2], were observed. The level of non-divergence west of the new low has dropped to near 700 mb. The convergence at 500 mb was observed in areas where strong cold advection was occurring. In the cases studied this convergence was almost always associated with the cold advection and not the pressure patterns.

Figures 10 and 11 depict the divergence patterns for

12Z 18 March. These patterns and those of 19 March are typical of moving-intensifying low pressure systems. The differences in the patterns depicted in the cross sections for this period are due to the orientation and location of the cross sections.

At the surface and the 850-mb levels at 12Z 18 March, large magnitude (greater than 100 x 10^{-7} per second) values of convergence and divergence were oriented symmetrically about the trough. Intense low level cold advection occurring to the southwest of the low at these levels was associated with the large divergence centers in that area. Likewise the convergence centers to the east of the low at these levels was associated with the warm advection occurring there. At 500 mb convergence and divergence centers of nearly equal magnitude were observed. At 300 mb the divergence to the east was greater than the convergence observed to the west of the trough. In cross section figure 18a, the column of convergence was again evident. At this time the magnitude of the convergence had increased over that observed at 00Z 17 March and there was significant deepening and intensification occurring.

Figures 12 and 18 depict the patterns for 00Z 19 March. These patterns are similar to those of 12Z 18 March.

By 12Z 19 March the surface low center had reached its minimum central pressure. Figure 13 illustrates the low level patterns for this time. At the surface the divergence

and convergence centers have migrated away from the trough but have maintained the same magnitudes. At 500 mb and 300 mb, figure 14, the line of zero divergence is now oriented east-west through the low center. In the cross section of vertical velocity, figure 19b, increased magnitudes were observed. Upward velocities are at least two times as large as those observed with the non-intensifying case.

B. BLOCKING HIGH

The second case represents a blocking high with associated cut-off lows. A well developed block existed over the eastern Atlantic and western European area during the middle of February, 1964. The divergence patterns on 13 February are presented as examples of this situation.

At 00Z 13 February, the block was well developed at all levels, the high and associated lows extending from the surface to at least 300 mb. At 850 mb, figure 20a, a pattern of moderate convergence to the east and divergence to the west existed about the lows. Divergence of small magnitude existed about the 850-mb high center. At 500 mb, figure 20b, the magnitude of divergence was even smaller than at 850 mb (less than 10×10^{-7} per second) and the pattern quite disorganized. Figure 21a, the 300-mb plan view, depicts a pattern of convergence and divergence about the lows which is reversed from the lower levels. Again, as at the other levels, divergence magnitudes about the high itself were small. Figure 22 depicts the cross section of divergence for this period. The troughs and ridge were all nearly vertical. Convergence (divergence) was observed east (west) of the lows at the lower levels while the configuration was reversed above 500 mb. Low level divergence was observed in the high center. The low level convergence observed east of the surface high is the result of a weak trough and associated frontal system traversing the northern

portion of the block.

Vertical motion patterns, figure 23, are relatively simple. The blocking high was located in an area of weak decending motion.

C. MIGRATORY COLD RIDGE

The third synoptic situation considered was a moving surface high pressure ridge associated with a cold air outbreak. The parent high pressure cell, central pressure 1049 mb, was centered to the east of Fairbanks, Alaska. Throughout the period studied, this cell remained quasi-stationary with the central pressure fluctuating between 1040-1050 mb. The surface pressure ridge, orientated in a north-south direction through Colorado on 20 March, retained its basic configuration and strength during its eastward movement. By 23 March, the surface pressure ridge was located in the upper Mississippi Valley. The cold front in this outbreak moved as far south as Guantanamo Bay, Cuba. Patterns of divergence similar to those observed with this system were observed with the other cold air outbreaks during February and March.

Height and divergence patterns for 12Z 20 March appear in figure 24. An intense low level divergence center, magnitude greater than 100 x 10^{-7} per second, was orientated in a north-south direction over the eastern half of the surface ridge. Convergence, associated with southerly flow and a low pressure system entering the Washington coast was observed to the west. At 300 mb, upper level convergence overlays the surface ridge. Divergence about the Canadian high center is small, but the typical patterns of low level divergence and upper level convergence were apparent. In

the cross section, figure 25a, terrain effects over the Rocky Mountains were evident. The areawise extent of the upper level convergence was also noticeable on this cross section.

Twelve hours later, figure 26, the surface ridge has impinged farther into the south-central United States. The magnitude of divergence had decreased slightly. Low level divergence, overlain by high level convergence, predominates over the surface pressure ridge. The closed 1045-mb Canadian high has small low level divergence and upper level convergence magnitudes. Large areawise extent of upper level convergence was observed.

At 00Z 22 March, figure 28, essentially the same divergence patterns were observed. A cross section of vertical velocity, figure 31b, depicted downward motion at all levels from the surface to 300 mb.

Figure 29 illustrates the divergence pattern for 12Z 22 March.

Figure 30 depicts the situation at 00Z 23 March. The strongest divergence centers have moved southeastward over the Atlantic Ocean following the advection maxima. The closed parent high pressure cell, center pressure of 1044 mb, has the low level divergence overlain by the high level convergence. The patterns in plan view remain the same about the surface pressure ridge.

5. Thermal Advection.

Thermal advection for the entire period was not computed because of data limitation; however, patterns of thermal advection with the divergent and non-divergent winds were studied for the period 00Z 13 February until 00Z 16 February 1964. The patterns of 00Z 14 February will be illustrated. Thermal advection with the non-divergent wind is plotted in degrees Centigrade per hour and thermal advection with the divergent wind is plotted in degrees Centigrade per hour x 10^2. Patterns of advection over mountainous regions and sparce data areas were considered to be unrepresentative. Thermal advection at the terrain level was not computed.

The surface pressure analysis for 00Z 14 February is shown in figure 32a. A low pressure system was centered northeast of Lake Ontario with a trough extending south to Mobile, Alabama. A moderately strong high was oriented north-south from Lake Superior to Texas. Figures 33a and 33b depict the 500 and 300-mb height patterns.

At the 850-mb level, figure 34a, cold advection was observed to the west of the trough while warm advection dominated the western portion of the ridge over the central United States. Magnitudes here were of the order of .2C per hour. Thermal advection with the divergent wind, figure 34b, also was negative to the west of the trough. The magnitude, however, was less than one-half of that found with

the non-divergent wind. The warm advection found at 850 mb over the western portion of the ridge was not observed at this level.

At 700 mb, figure 35, the patterns were similar to those at 850 mb but the magnitudes were smaller. The patterns of cold advection associated with the trough were displaced westward with the tilt of the trough. As at 850 mb the area of warm advection found in the ridge with the non-divergent wind is not observed with the divergent wind.

Thermal advection with the non-divergent wind at 500 mb, figure 36a, showed a large area of weak cold advection to the east of the 500-mb trough. Weak warm advection was associated with the ridge. With the divergent wind, figure 36b, warm advection was observed east of the trough and very weak cold advection observed with the ridge. This change in sign was associated with the change in sign of the divergence patterns from the 700-mb level to the 500-mb level. Magnitudes of non-divergent wind thermal advection were 10 times those observed with the divergent wind.

Figure 37 depicts thermal advection with the divergent wind at 300 mb. The patterns and sign are similar to those found at 500 mb, however the magnitudes are equal to those found at 850 mb.

6. Summary.

Numerous cases of the three-dimensional distribution of velocity divergence in tropospheric pressure systems were studied. Typical patterns of velocity divergence associated with moving-non-intensifying low pressure systems are depicted by figures 6, 7, and 15. Significant features observed at this stage of the life cycle were: small magnitudes of divergence, less than 70 x 10^{-7} per second; symmetrical patterns of divergence about the trough line; and the level of minimum divergence being located approximately at the 500-mb level. Vertical velocities associated with this stage of the life cycle are upward to the east and downward to the west of the low, with maximum magnitudes near 20 x 10^{-4} mb per second. Vertical motion in a vertical column was generally of the same sign with maximum values occurring near 500 mb.

In the moving-intensifying low pressure system the most significant change was the increase in magnitude of divergence values over the non-intensifying system. Figures 10 and 11 show magnitudes as high as 160 x 10^{-7} per second. Also significant was the mid-tropospheric column of convergence and the increased lateral extent of the divergence centers. Maximum upward vertical velocities associated with this stage of the life cycle were as much as four times as great as those found in the non-intensifying system.

The blocking situation is characterized by small

magnitudes of divergence, near zero at the ridge line, and less than 60 x 10^{-7} per second in the cut-off lows. The orientation of the divergence centers about the lows is similar to that found in the non-intensifying low.

The moving surface high pressure ridge, or high pressure ridge associated with a cold air outbreak, is characterized by strong low level divergence overlain by strong high level convergence. Again, as in the intensifying low, magnitudes become greater than 100 x 10^{-7} per second. Moderate downward vertical motion, with maximum values found near 500 mb, existed east of the surface ridge.

In this study magnitudes of thermal advection with the non-divergent wind were usually more than four times as great as magnitudes associated with thermal advection with the divergent wind. The sign of the two types of advection usually agrees at low levels but is usually opposite at 500 and 300 mb.

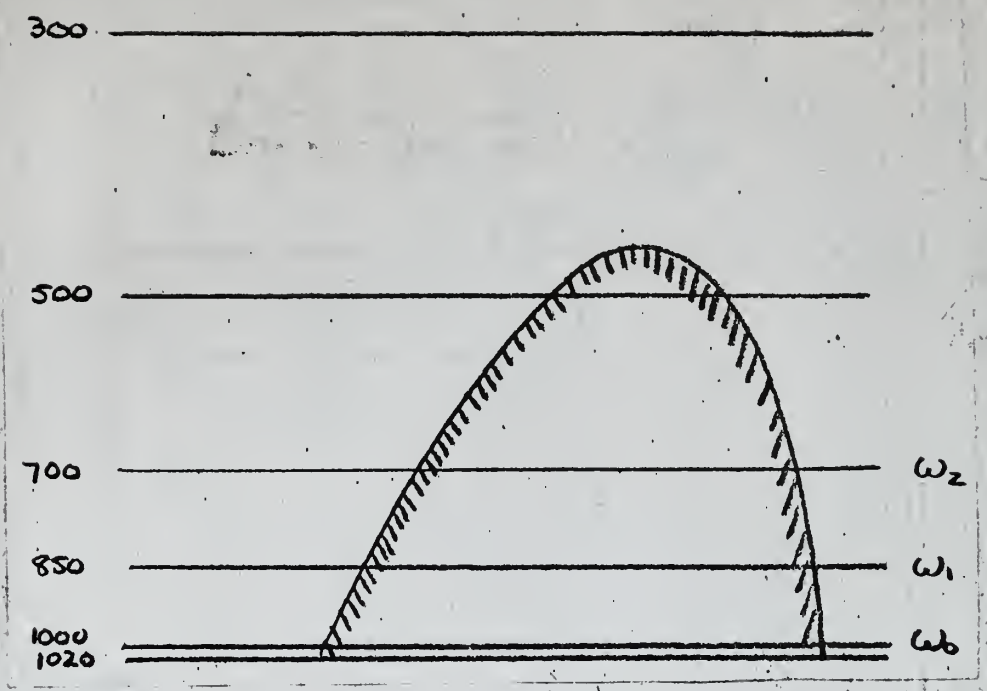

Figure 1a. Division of the atmosphere for the divergence computation at 1000 mb.

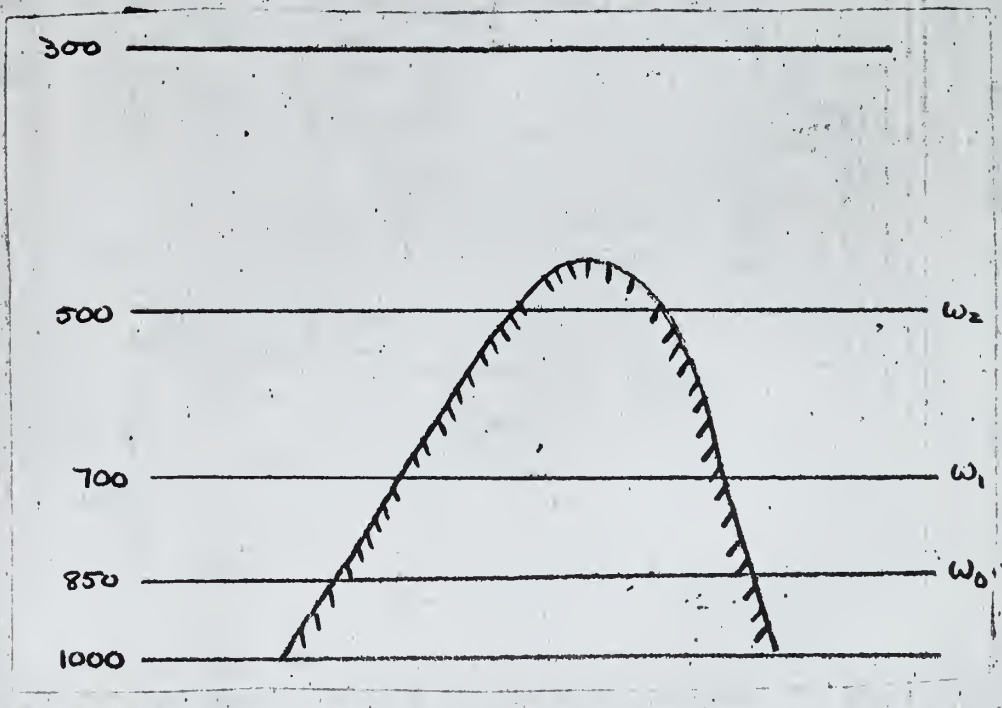

Figure 1b. Division of the atmosphere for the divergence computation at 850, 700, 500, and 300 mb.

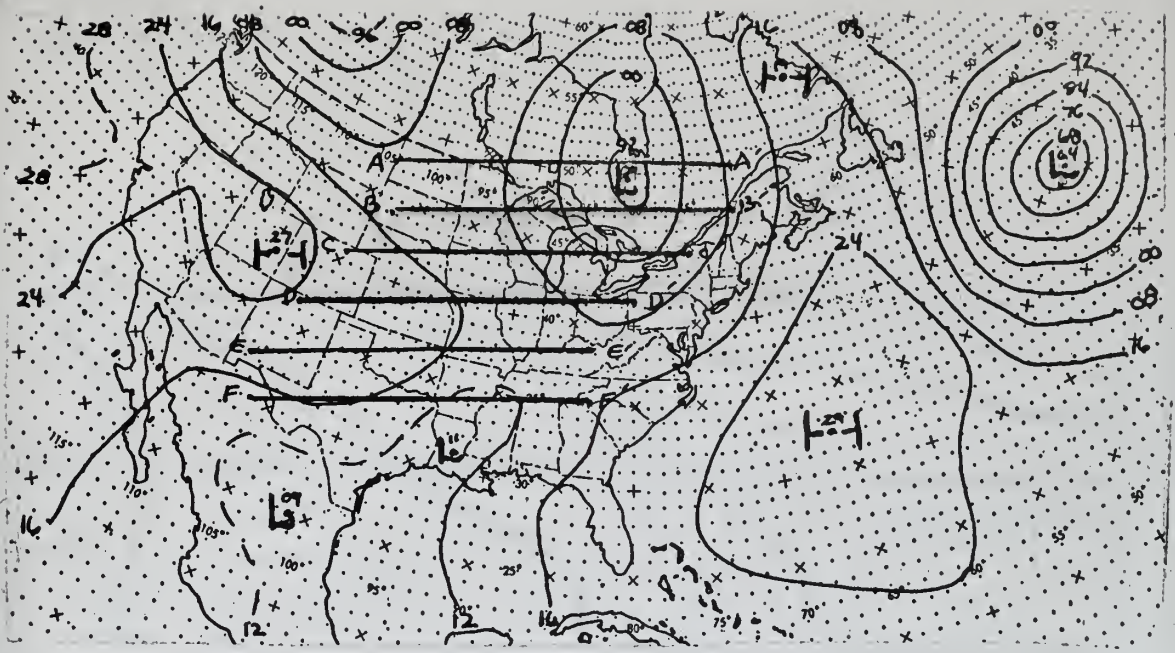

Figure 2a. Surface pressure analysis at 00Z 15 March, 1964 (16~1016 mb)

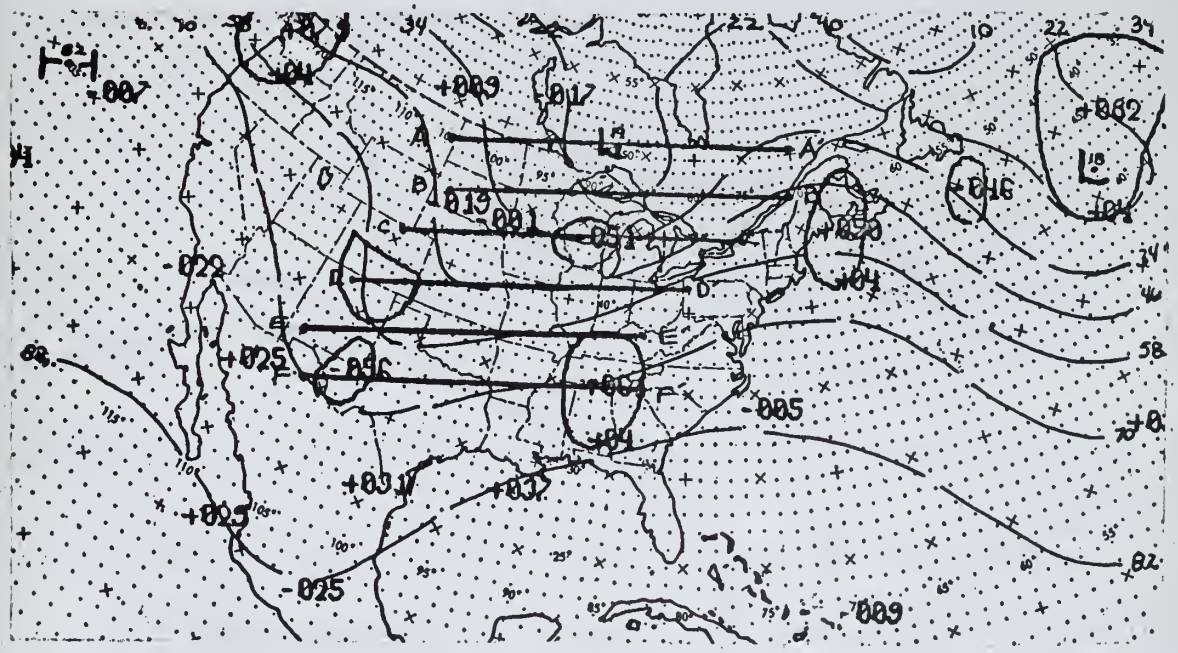

Figure 2b. 500-mb divergence in units of 10^{-7} per second and 500-mb analysis (34~5,340 meters) at 00Z 15 March 1964.

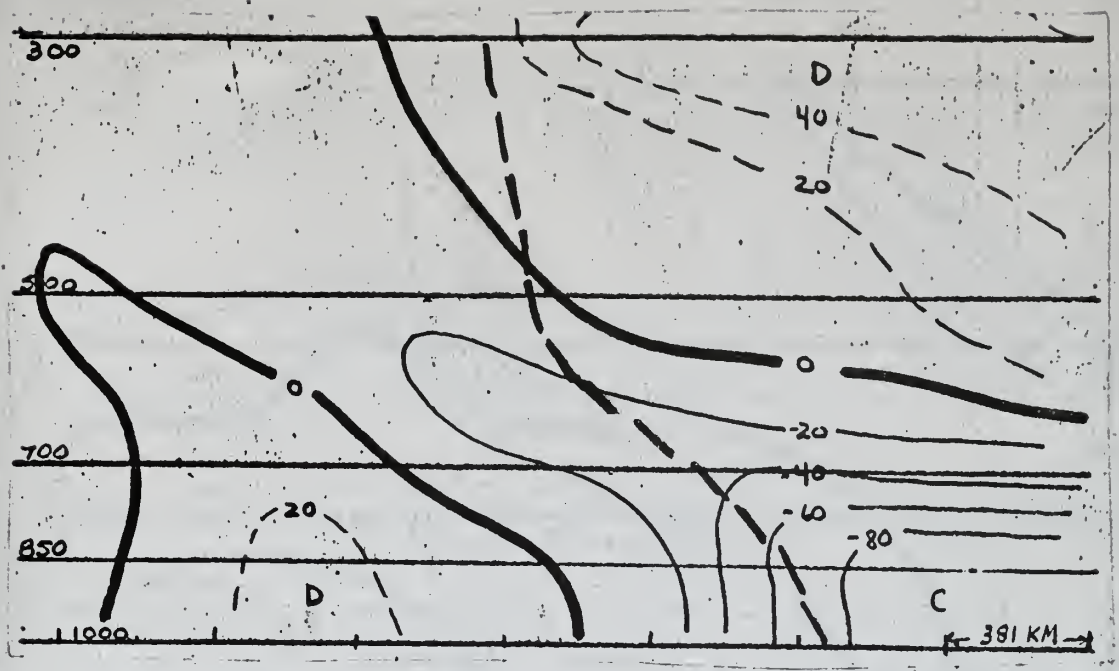

Figure 3a. Cross section of divergence in units of 10^{-7} per second taken along line AA' on figure 2. (00Z 15 March)

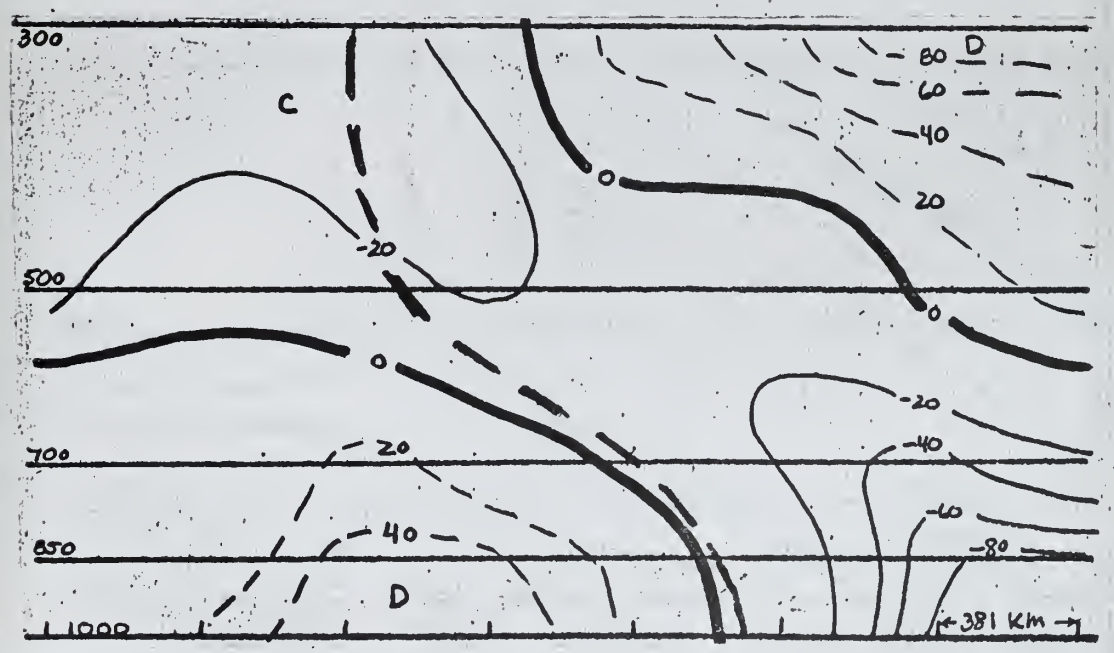

Figure 3b. Cross section of divergence in units of 10^{-7} per second taken along line BB' on figure 2. (00Z 15 March)

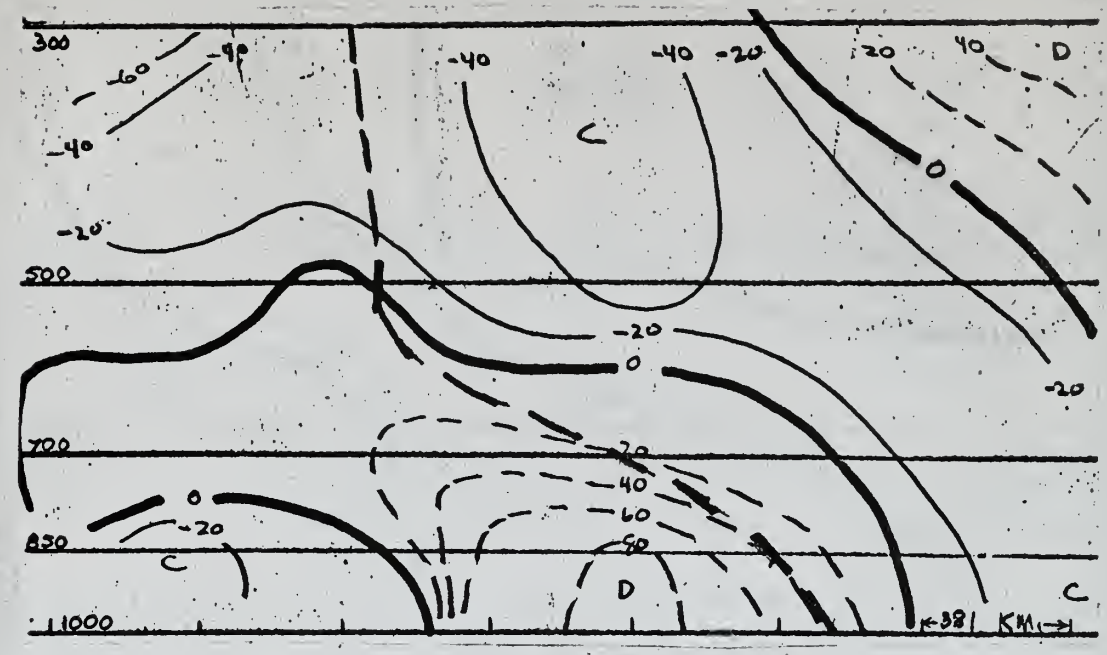

Figure 4a. Cross section of divergence in units of 10^{-7} per second taken along line CC' on figure 2. (00Z 15 March)

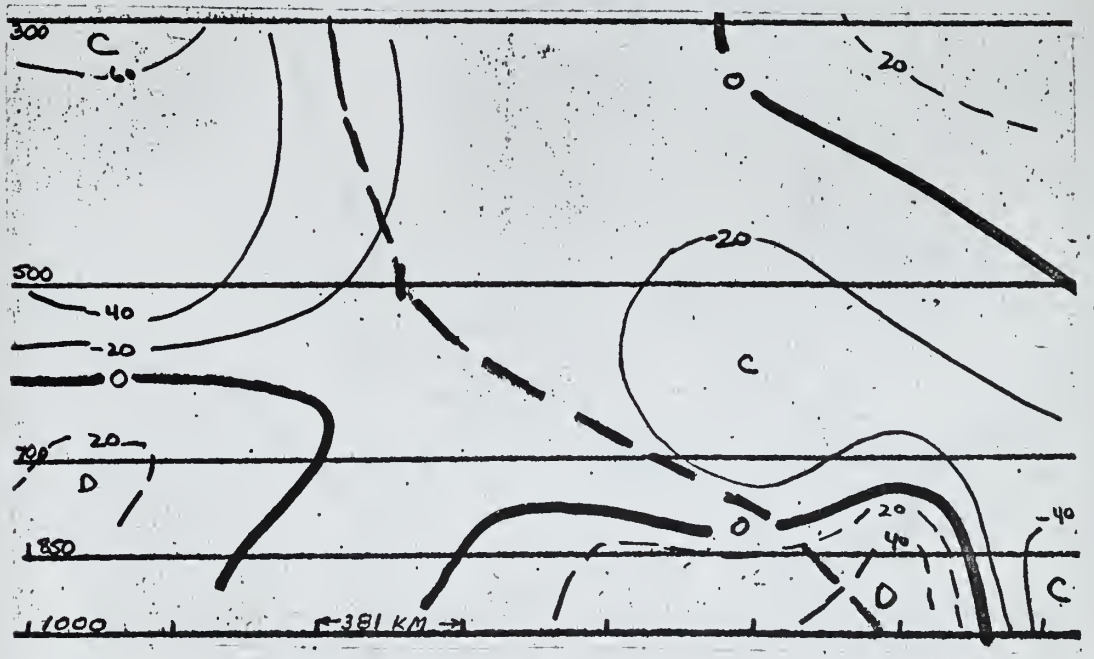

Figure 4b. Cross section of divergence in units of 10^{-7} per second taken along line DD' on figure 2. (00Z 15 March)

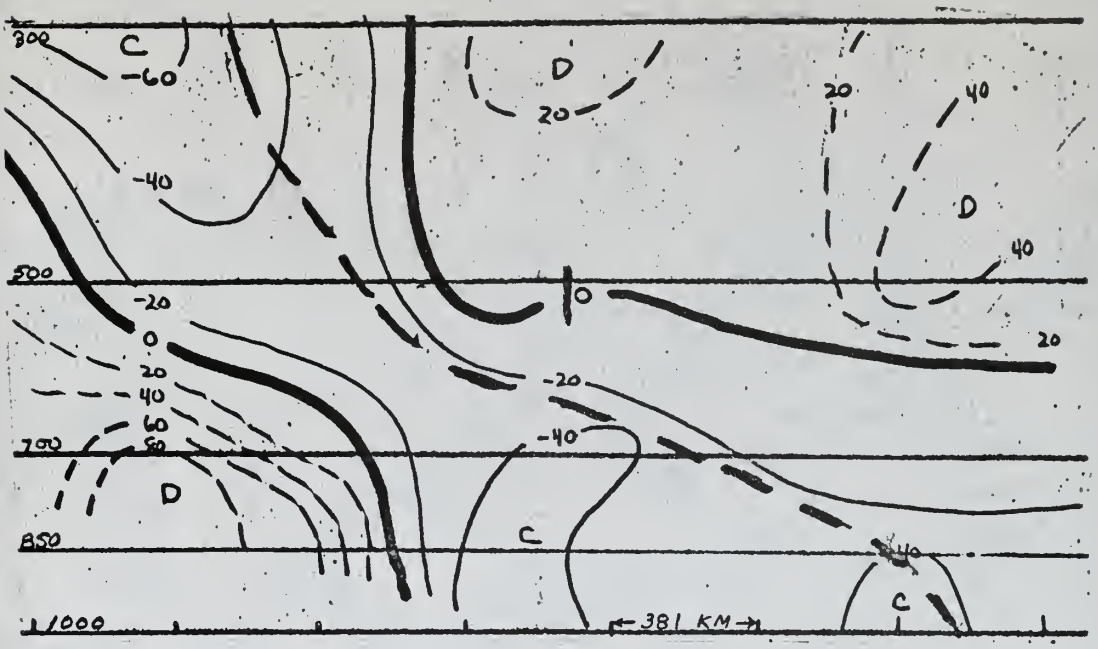

Figure 5a. Cross section of divergence in units of 10^{-7} per second taken along line EE' on figure 2. (00Z 15 March)

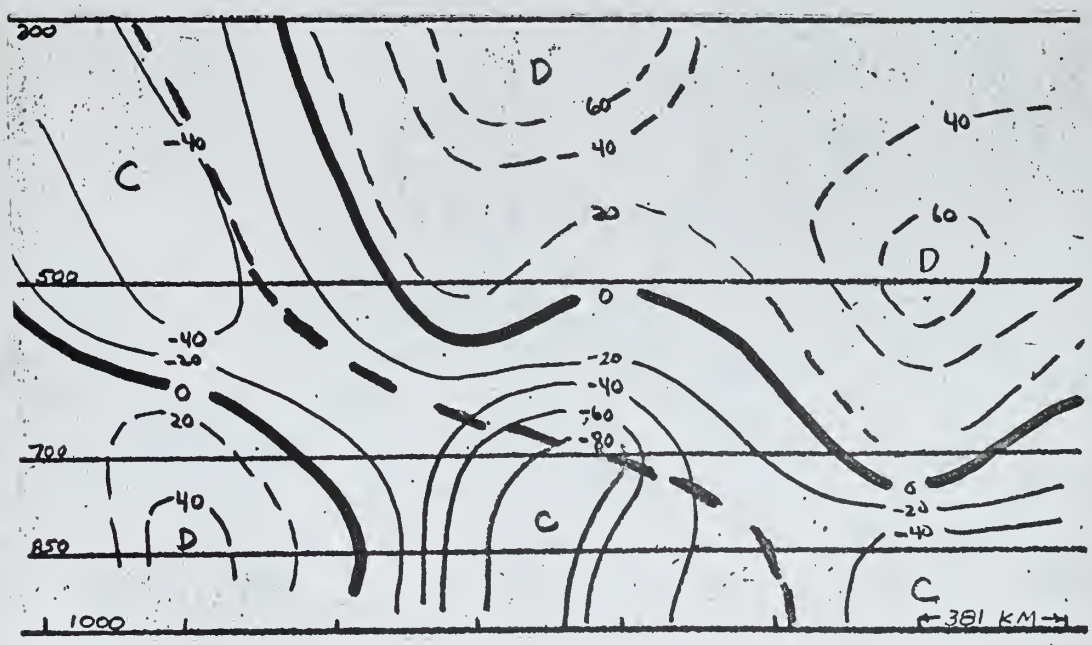

Figure 5b. Cross section of divergence in units of 10^{-7} per second taken along line FF' on figure 2. (00Z 15 March)

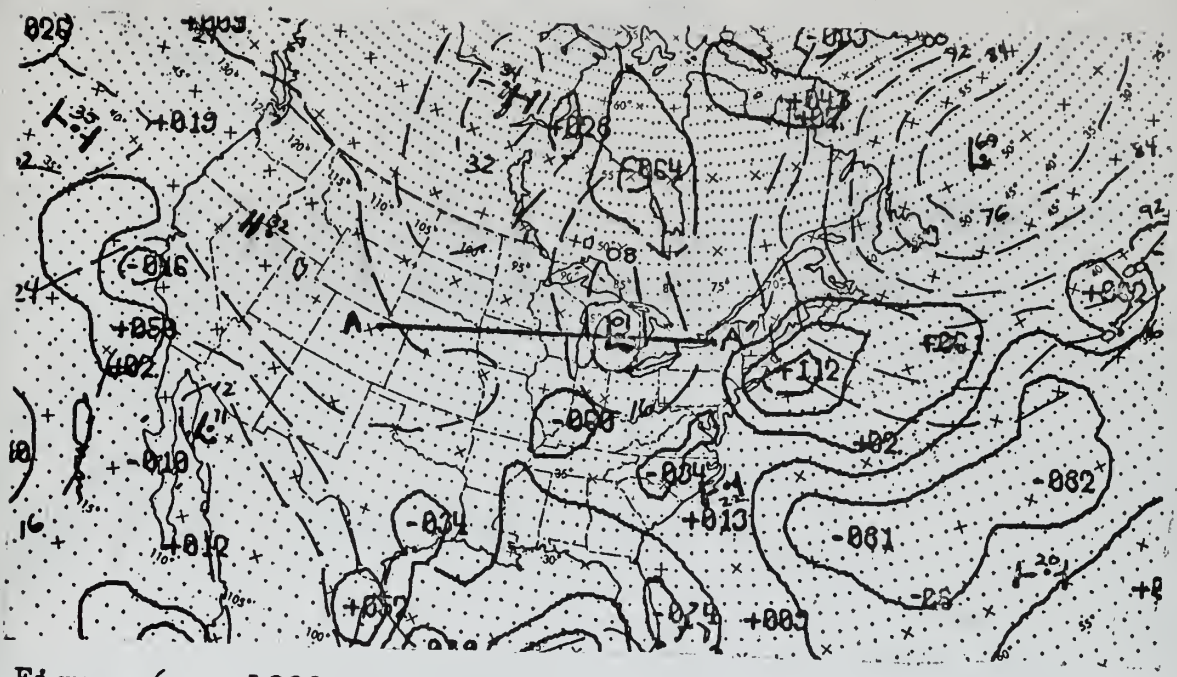

Figure 6a. 1000-mb divergence in units of 10^{-7} per second and surface pressure analysis (16 ~ 1016 mb) at 00Z 17 March 1964.

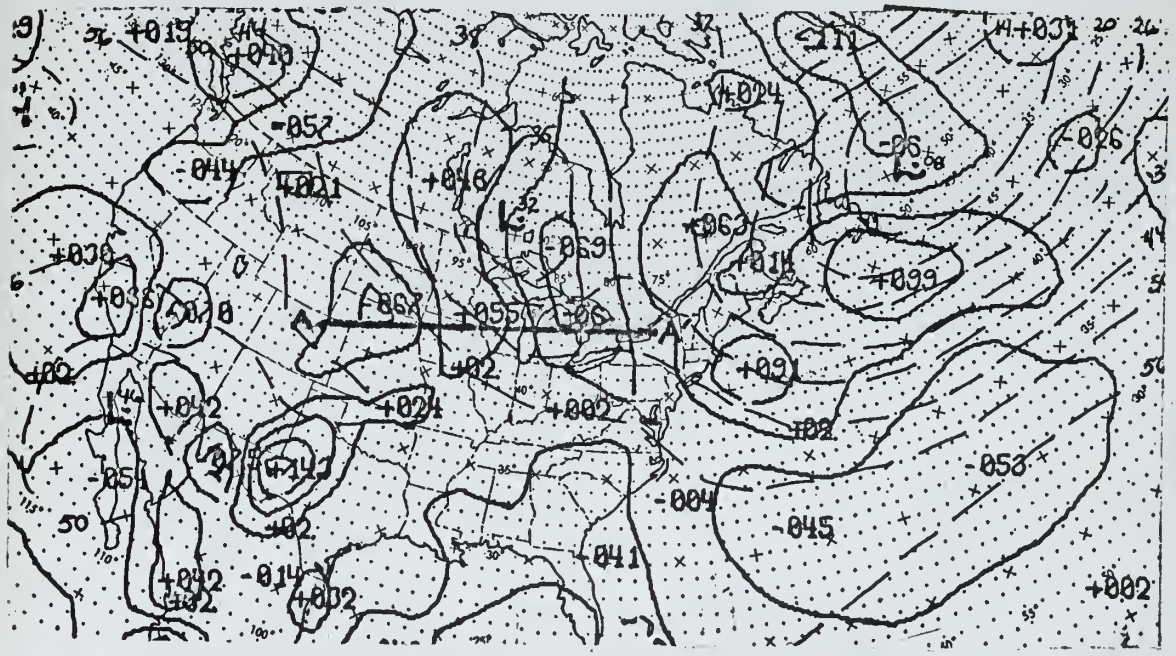

Figure 6b. 850-mb divergence in unit of 10^{-7} per second and 850-mb height analysis (50 ~ 1,500 meters) at 00Z 17 March 1964.

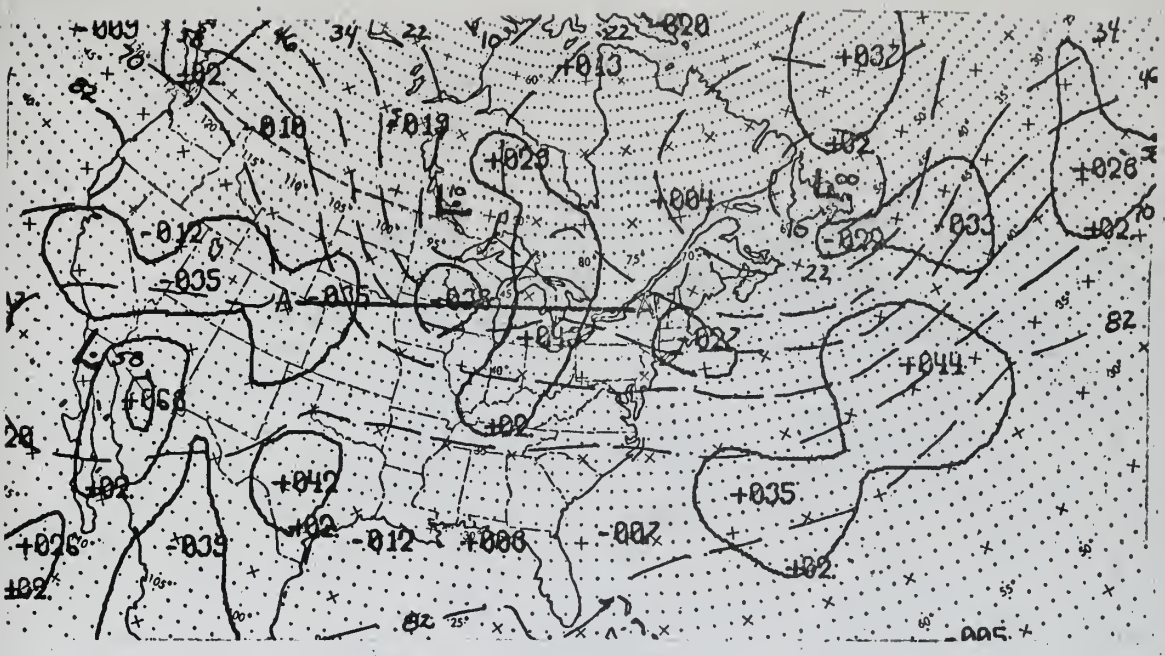

Figure 7a. 500-mb divergence in units of 10^{-7} per second and 500-mb height analysis (22~5,220 meters) at 00Z 17 March 1964.

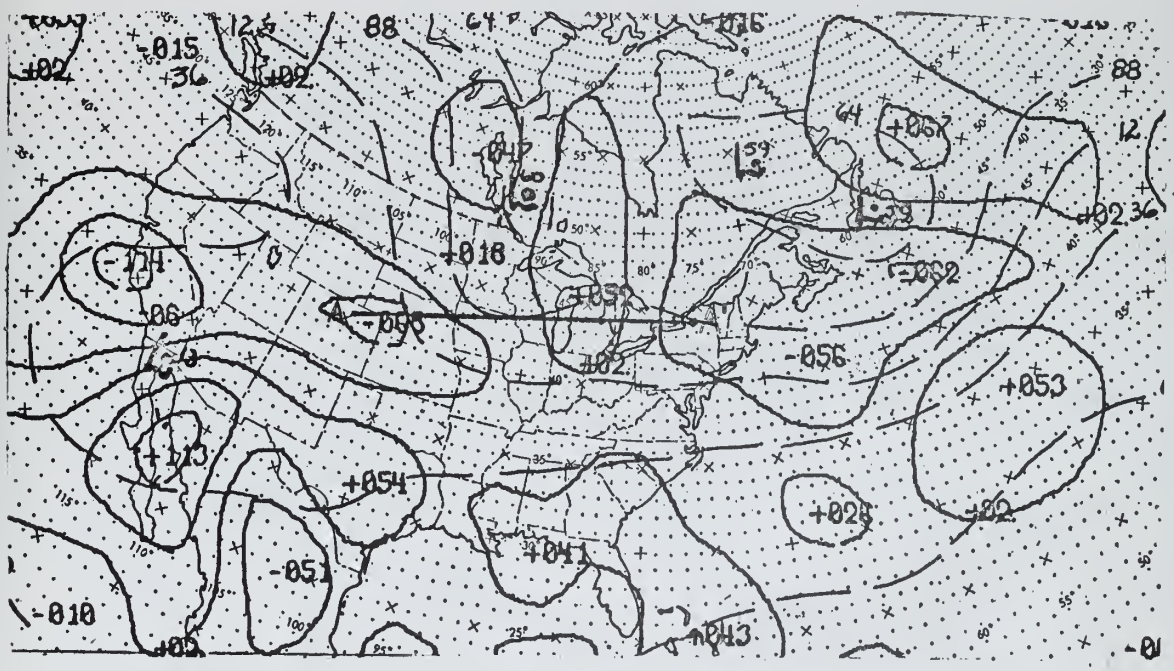

Figure 7b. 300-mb divergence in units of 10^{-7} per second and 300-mb height analysis (12~9,120 meters) at 00Z 17 March 1964.

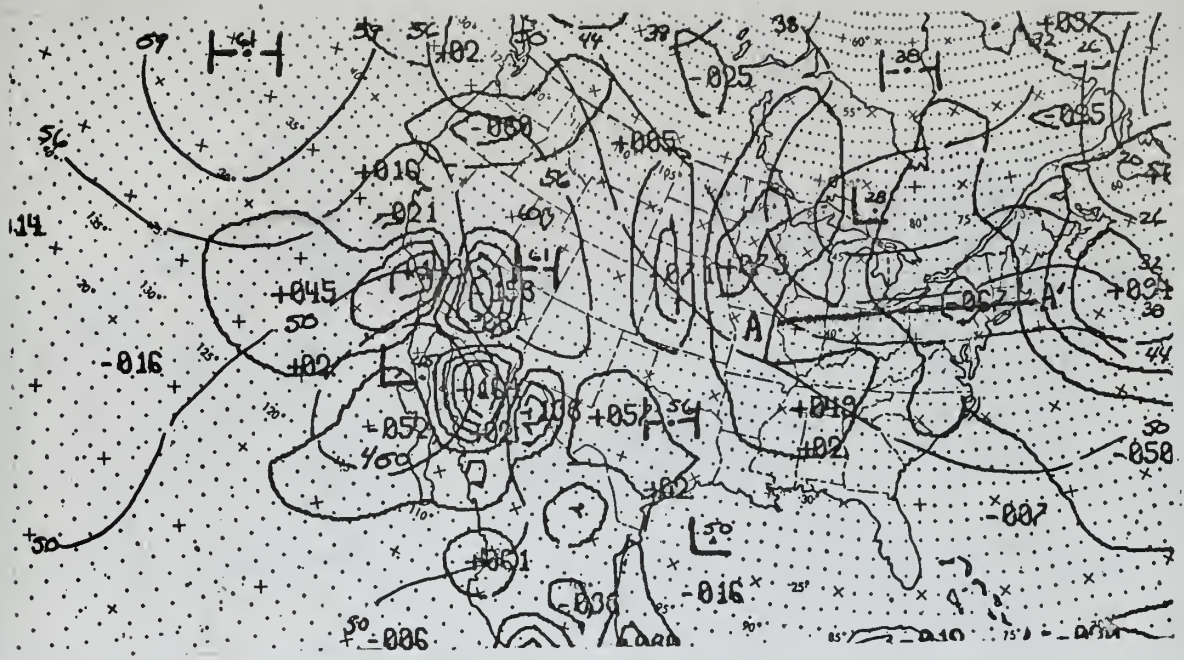

Figure 8a. 850-mb divergence in units of 10^{-7} per second and 850-mb height analysis (50~1500 meters) at 12Z 17 March 1964.

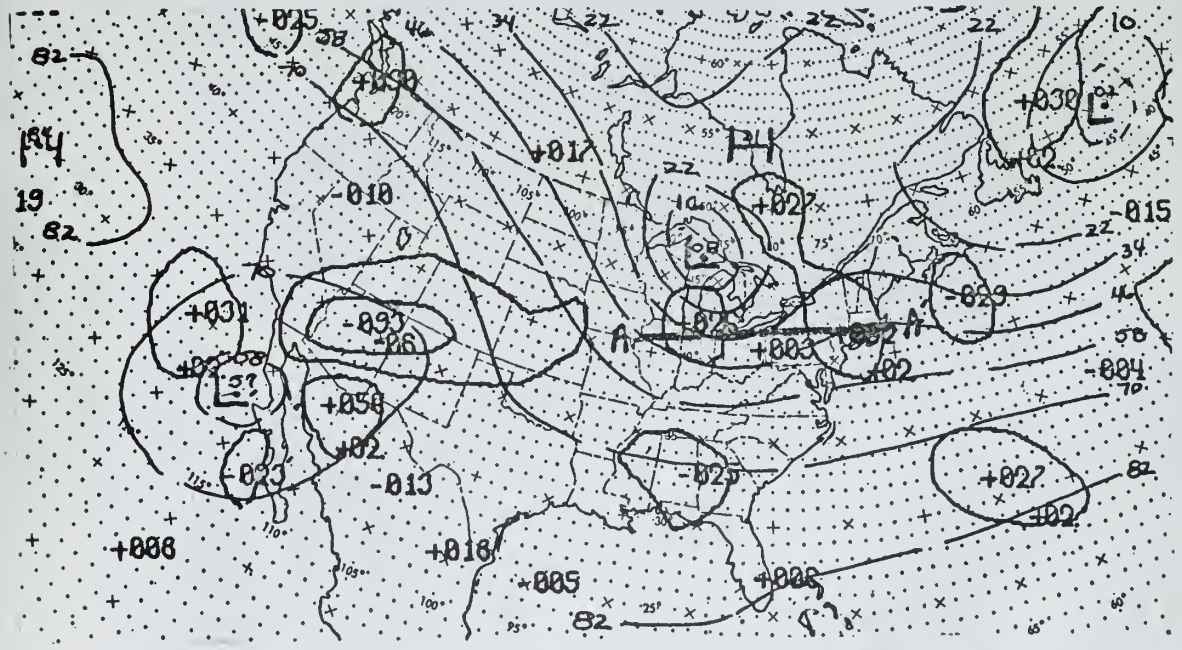

Figure 8b. 500-mb divergence in units of 10^{-7} per second and 500-mb height analysis (22~5,220 meters) at 12Z 17 March 1964.

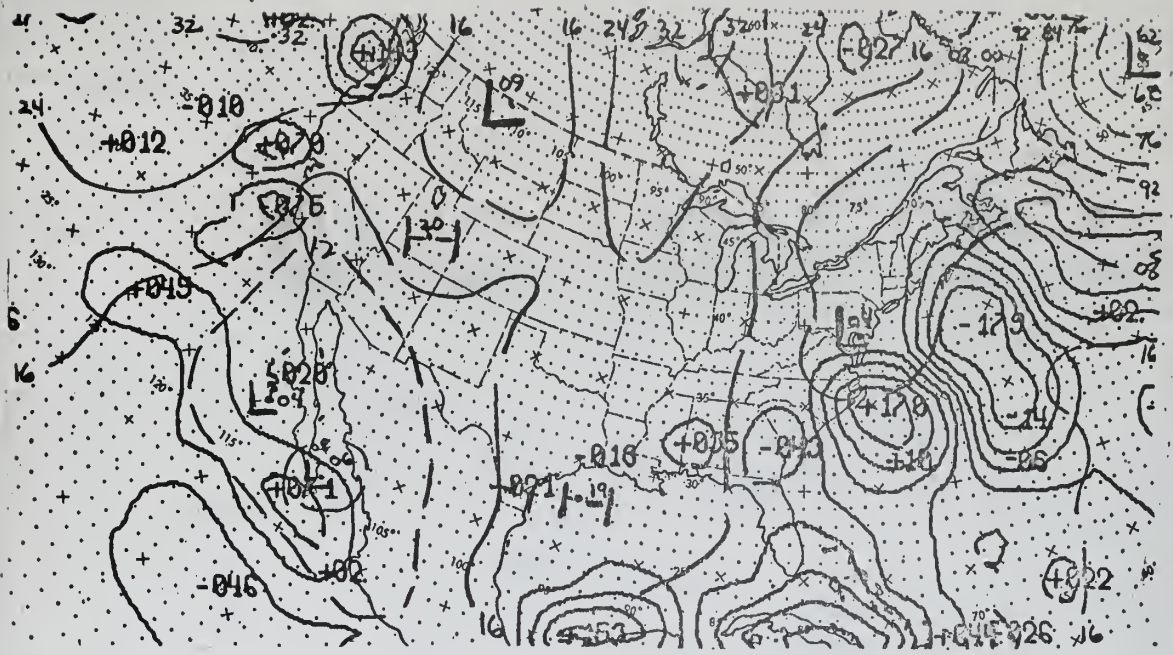

Figure 9a. 1000-mb divergence in units of 10^{-7} per second and surface pressure analysis (1032 mb~32) at 00Z 18 March 1964.

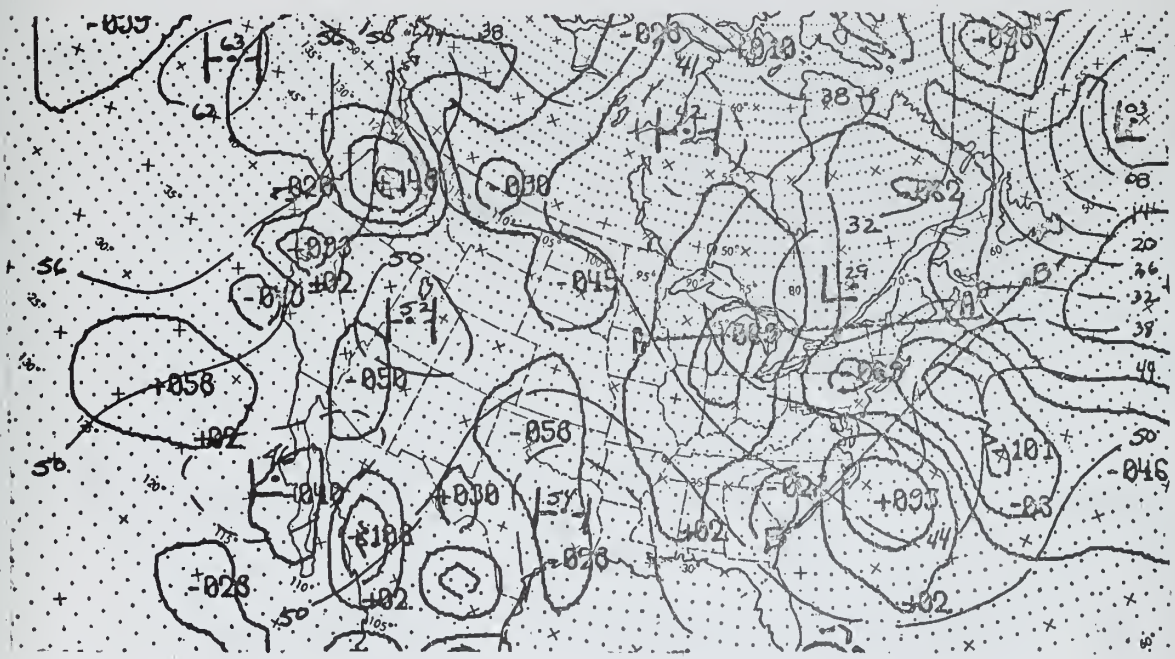

Figure 9b. 850-mb divergence in units of 10^{-7} per second and 850-mb height analysis (50~1,500 meters) at 00Z 18 March 1964.

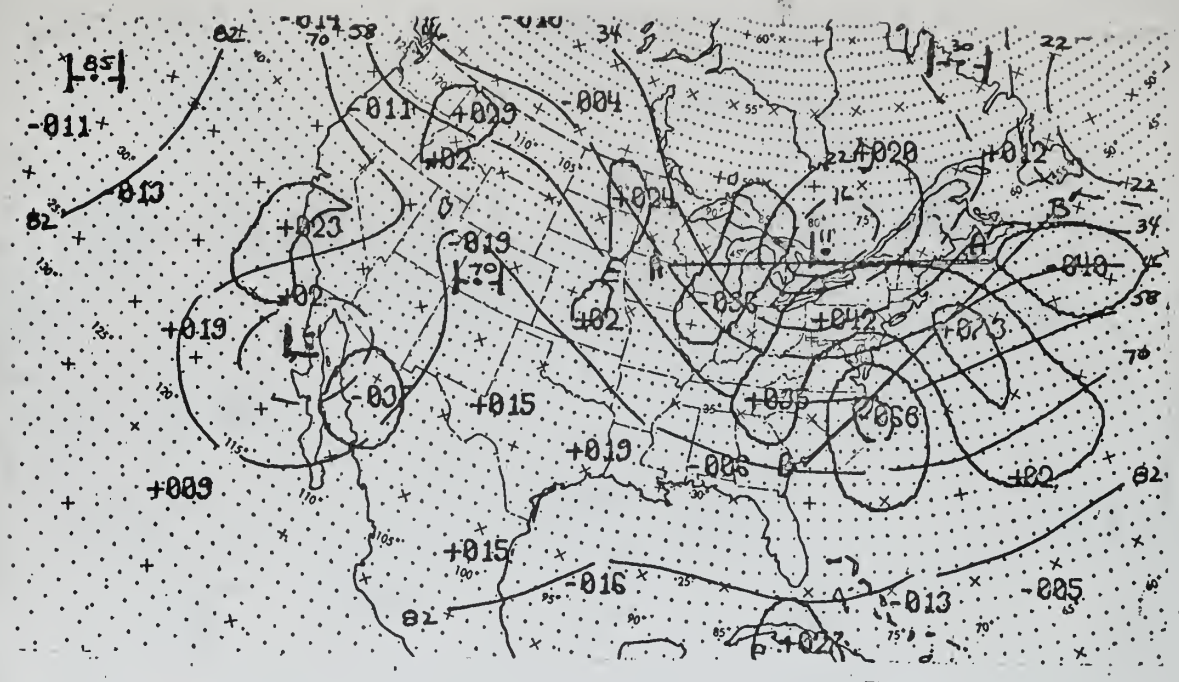

Figure 9c. 500-mb divergence in units of 10^{-7} per second and 500-mb height analysis (22~5,220 meters) at 00Z 18 March 1964.

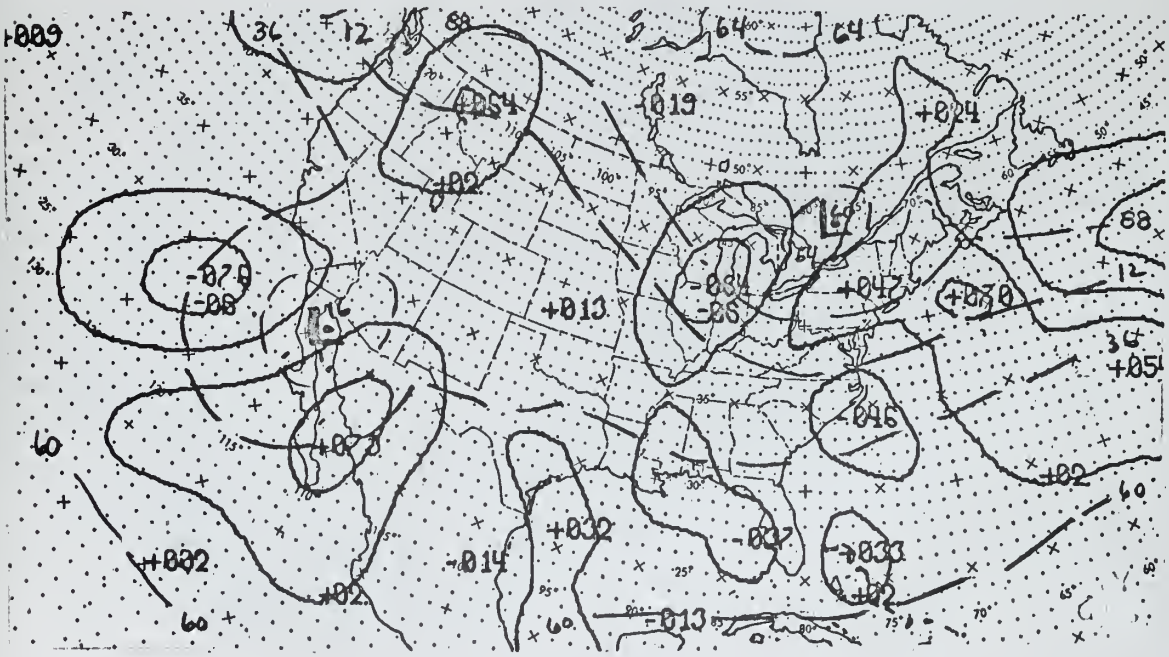

Figure 9d. 300-mb divergence in units of 10^{-7} per second and 300-mb height analysis (12~9,120 meters) at 00Z 18 March 1964.

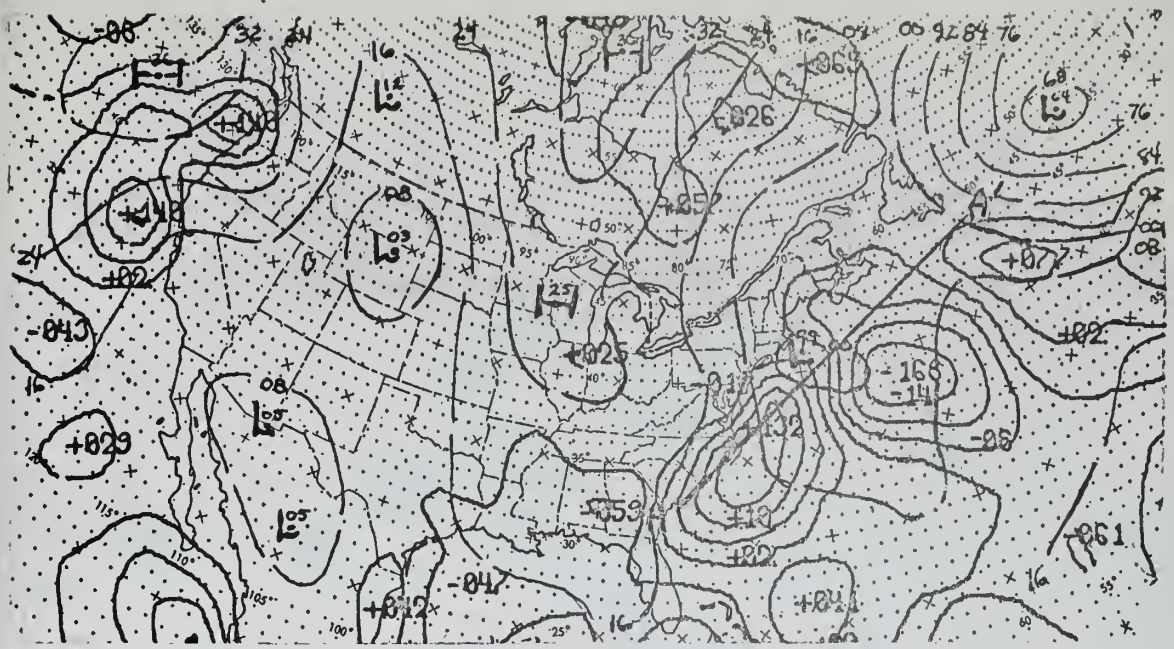

Figure 10a. 1000-mb divergence in units of 10^{-7} per second and surface pressure analysis (32~1032 mb) at 12Z 18 March 1964.

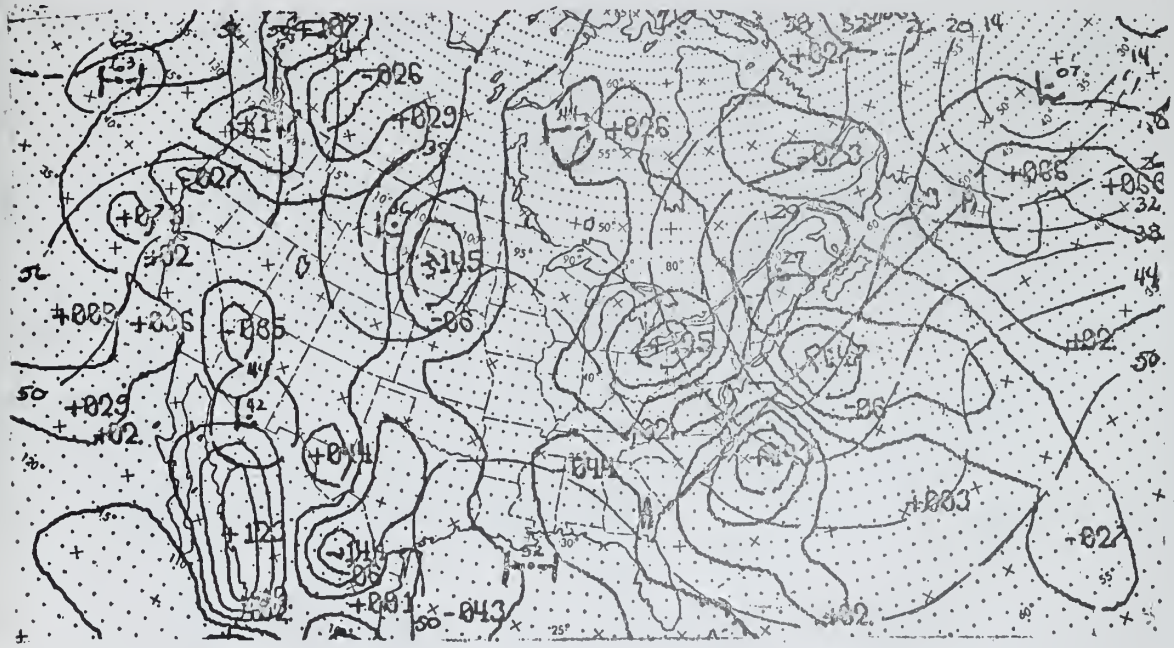

Figure 10b. 850-mb divergence in units of 10^{-7} per second and 850-mb height analysis (50~1,500 meters) at 12Z 18 March 1964.

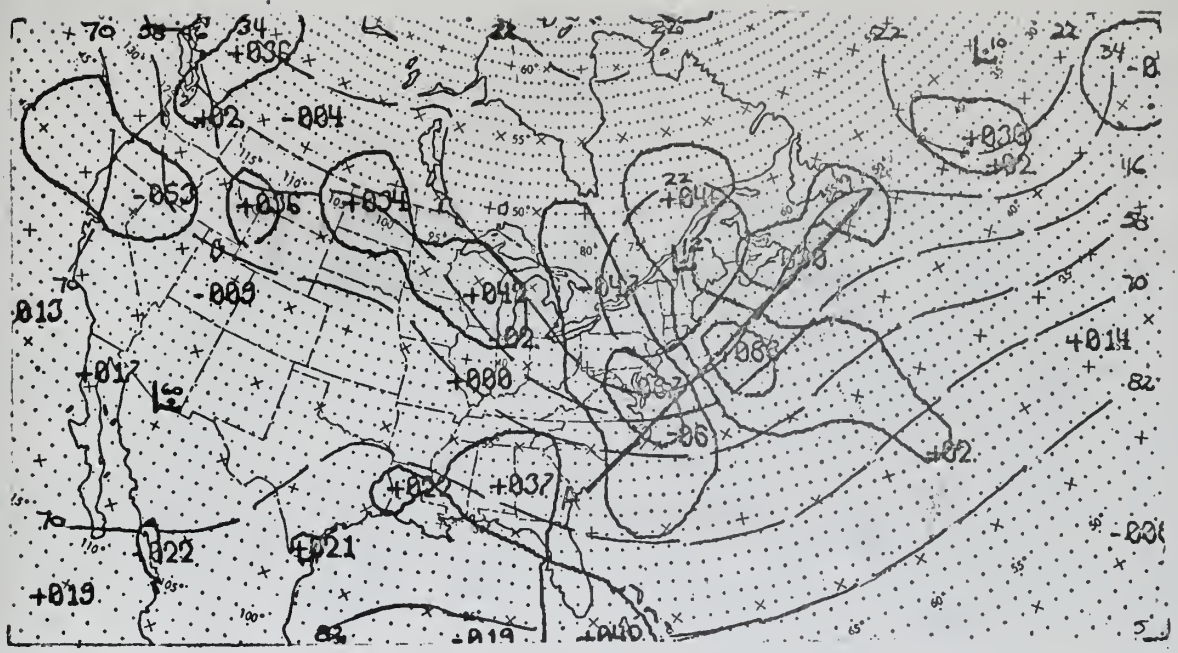

Figure 11a. 500-mb divergence in units of 10^{-7} per second and 500-mb height analysis (22~5,220 meters) at 12Z 18 March 1964.

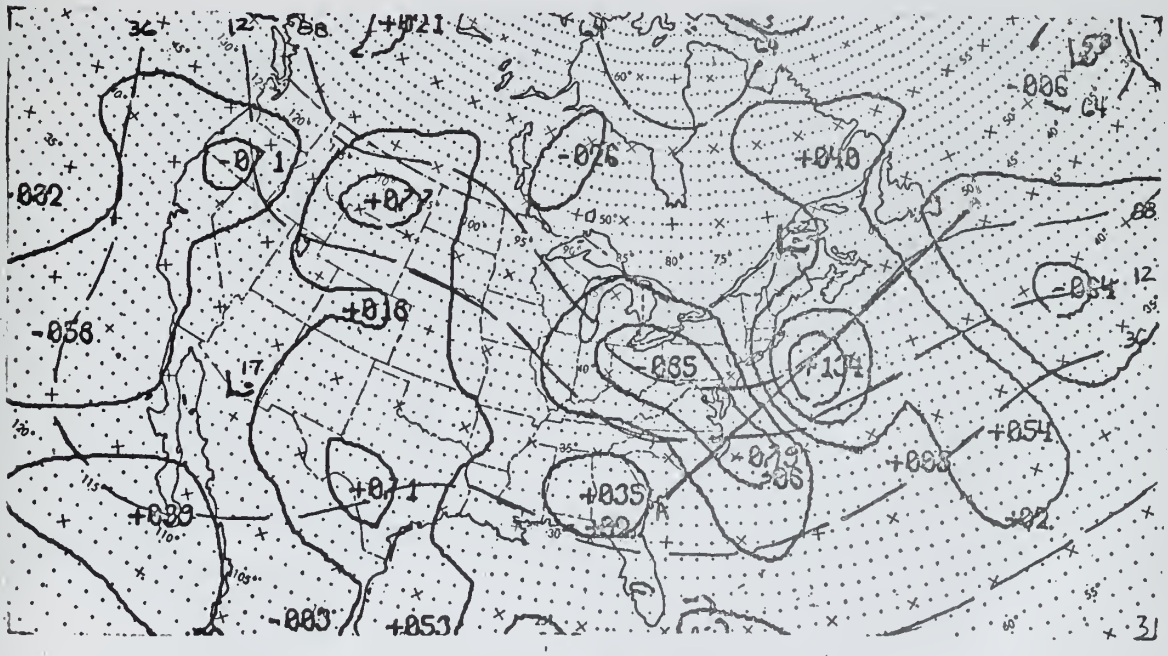

Figure 11b. 300-mb divergence in units of 10^{-7} per second and 300-mb height analysis (12~9,120 meters) at 12Z 18 March 1964.

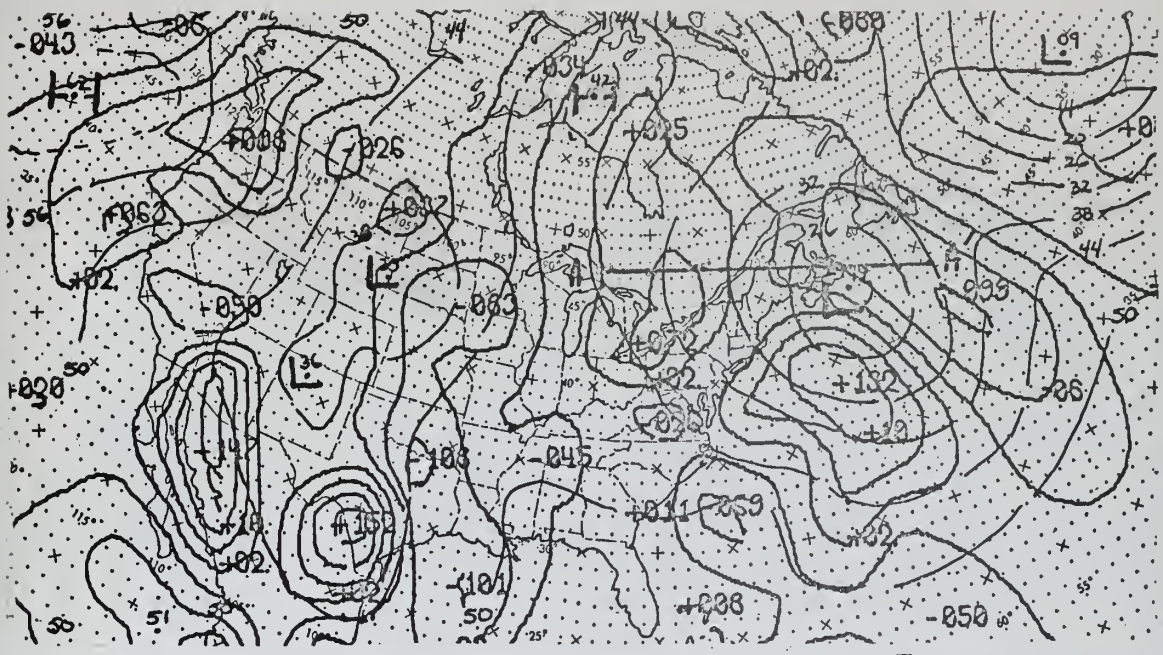

Figure 12a. 850-mb divergence in units of 10^{-7} per second and 850-mb height analysis (50~1,500 meters) at 00Z 19 March 1964.

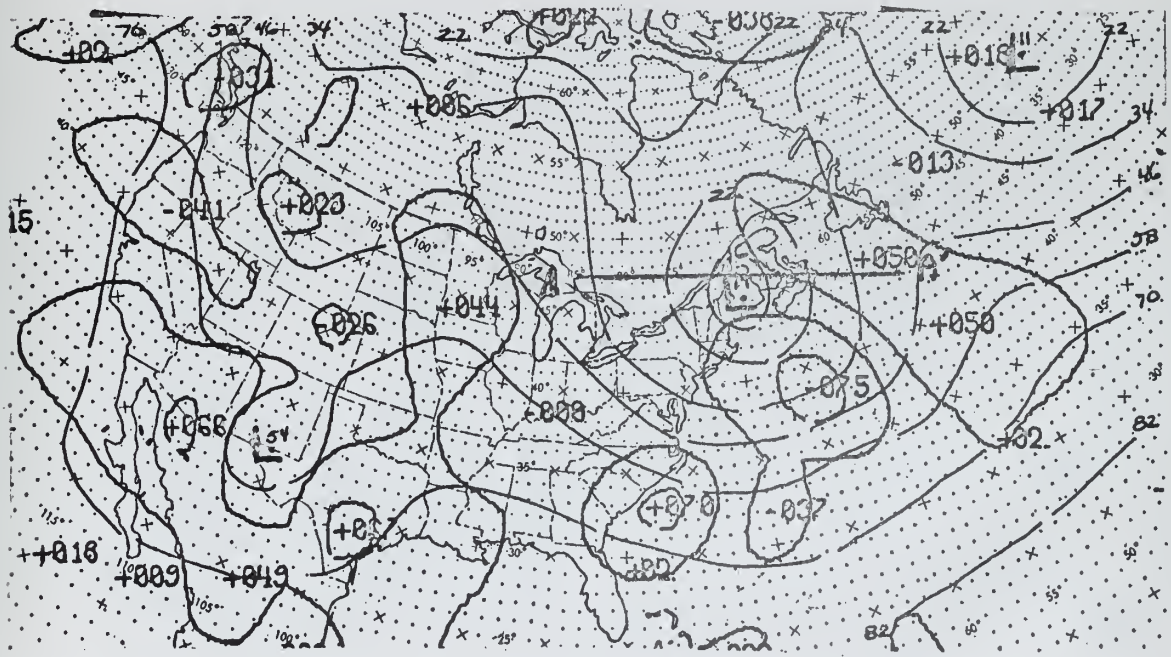

Figure 12b. 500-mb divergence in units of 10^{-7} per second and 500-mb height analysis (22~5,220 meters) at 00Z 19 March 1964.

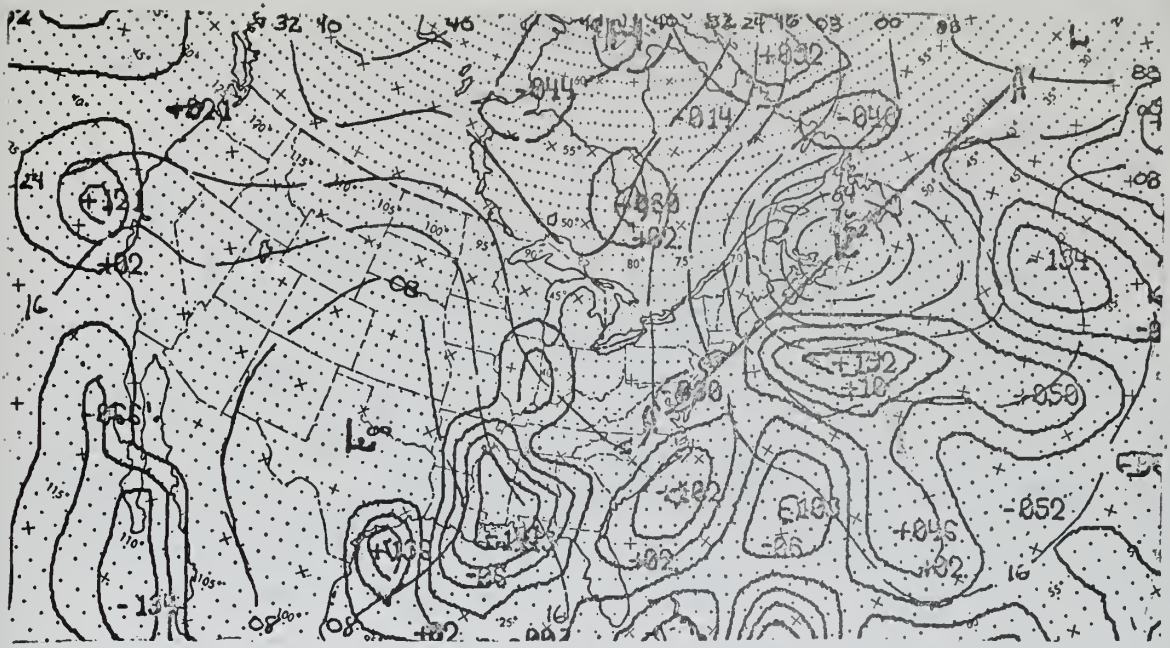

Figure 13a. 1000-mb divergence in units of 10^{-7} per second and surface pressure analysis (32~1032 mb) at 12Z 19 March 1964.

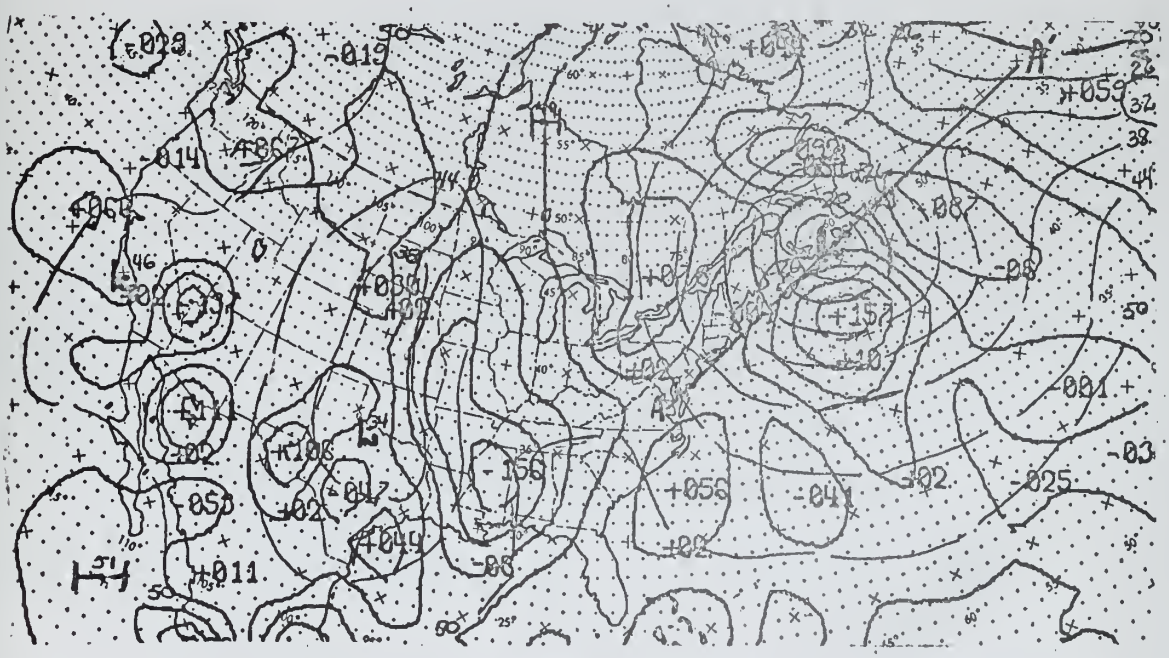

Figure 13b. 850-mb divergence in units of 10^{-7} per second and 850-mb height analysis (50~1,500 meters) at 12Z 19 March 1964.

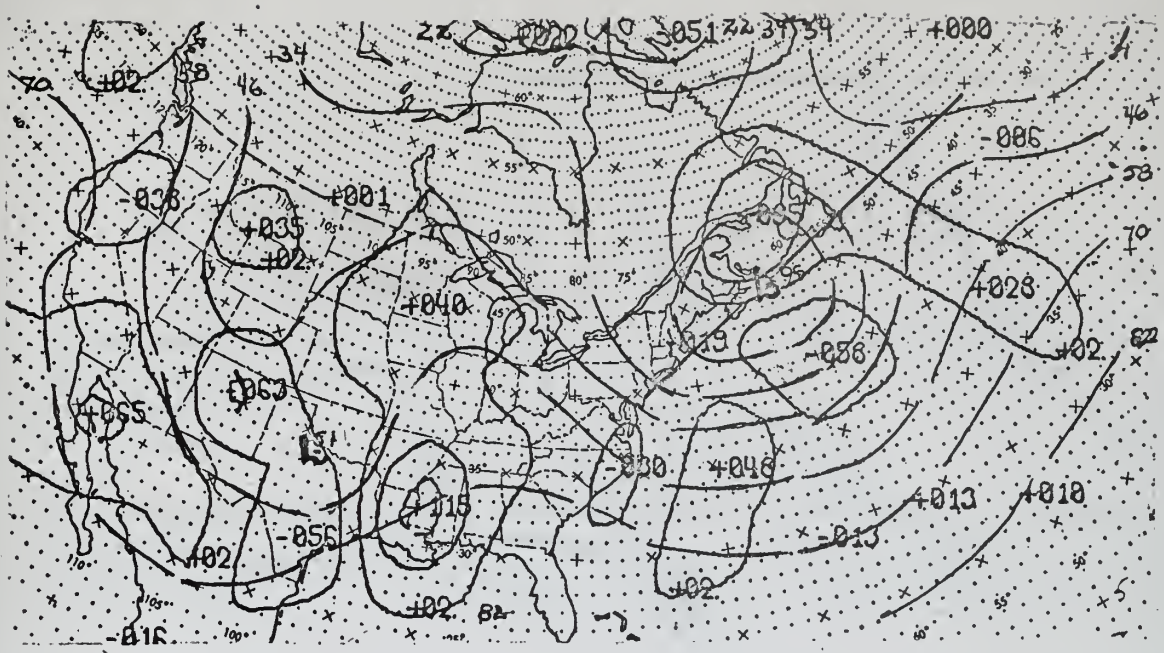

Figure 14a. 500-mb divergence in units of 10^{-7} per second and 500-mb height analysis (22~5,220 meters) at 12Z 19 March 1964.

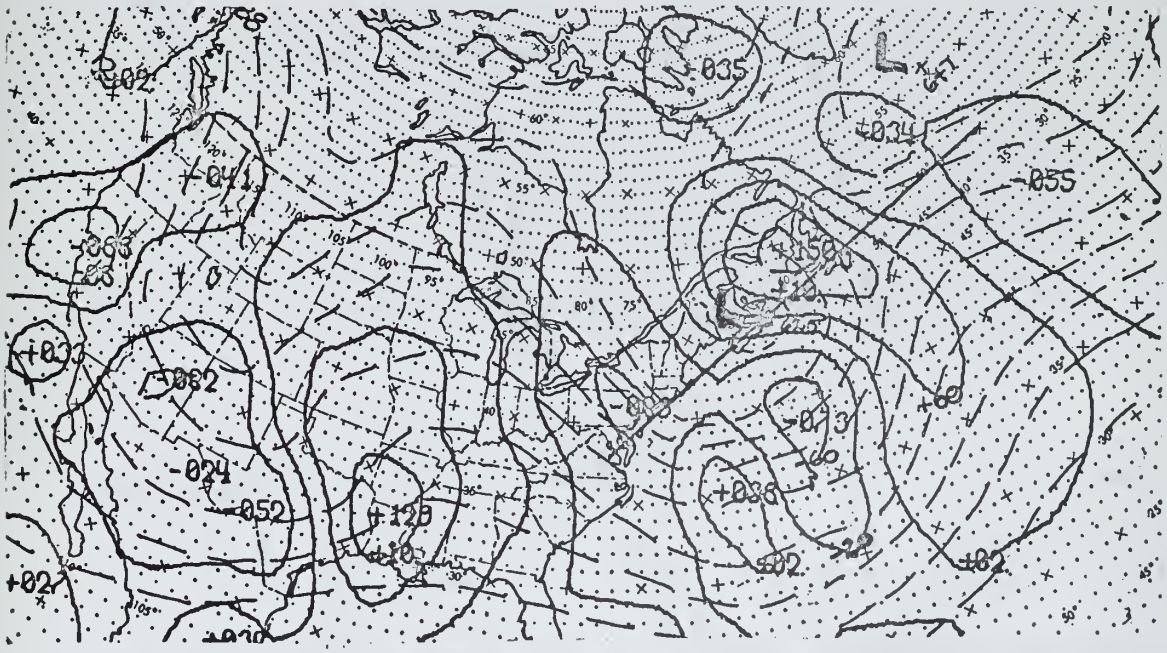

Figure 14b. 300-mb divergence in units of 10^{-7} per second and 300-mb height analysis (12~9,120 meters) at 12Z 19 March 1964.

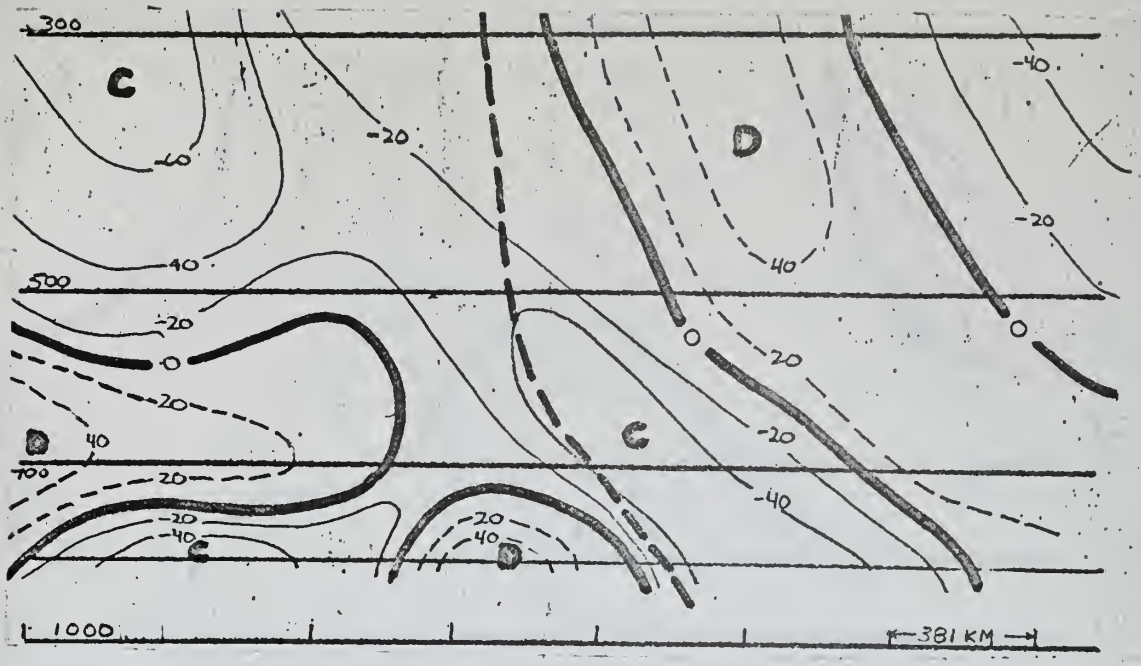

Figure 15a. Cross section of divergence in units of 10^{-7} per second taken along line AA' on figure 6a. (00Z 17 March)

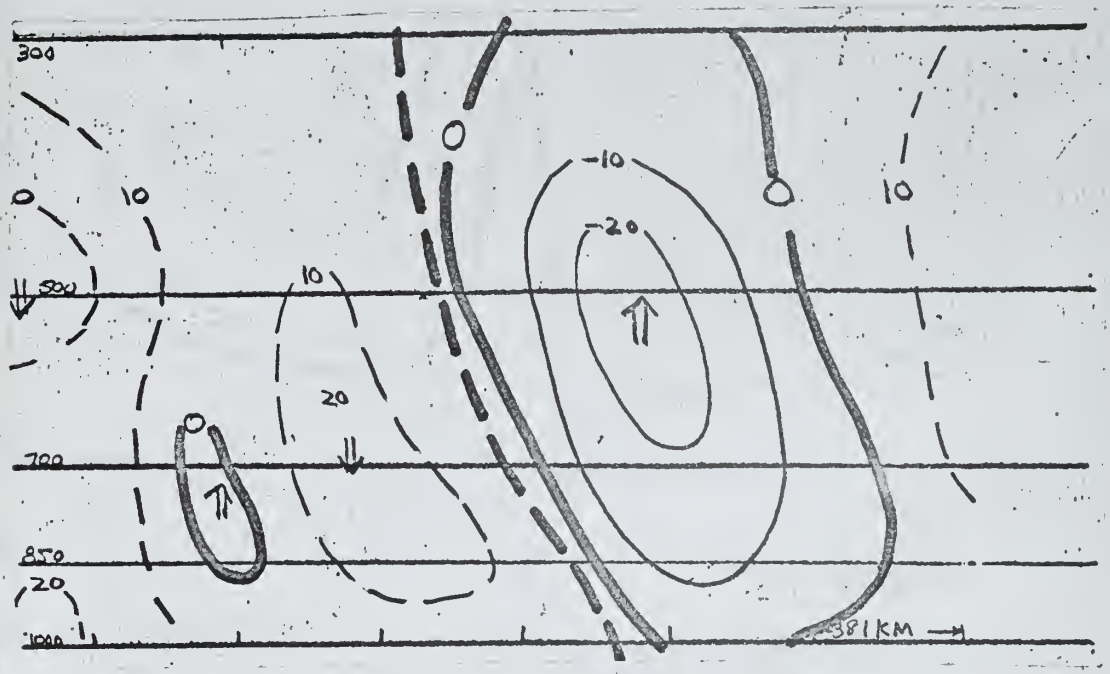

Figure 15b..Cross section of vertical velocity in units of 10^{-4} mb per second taken along line AA' on figure 6a. (00Z 17 March)

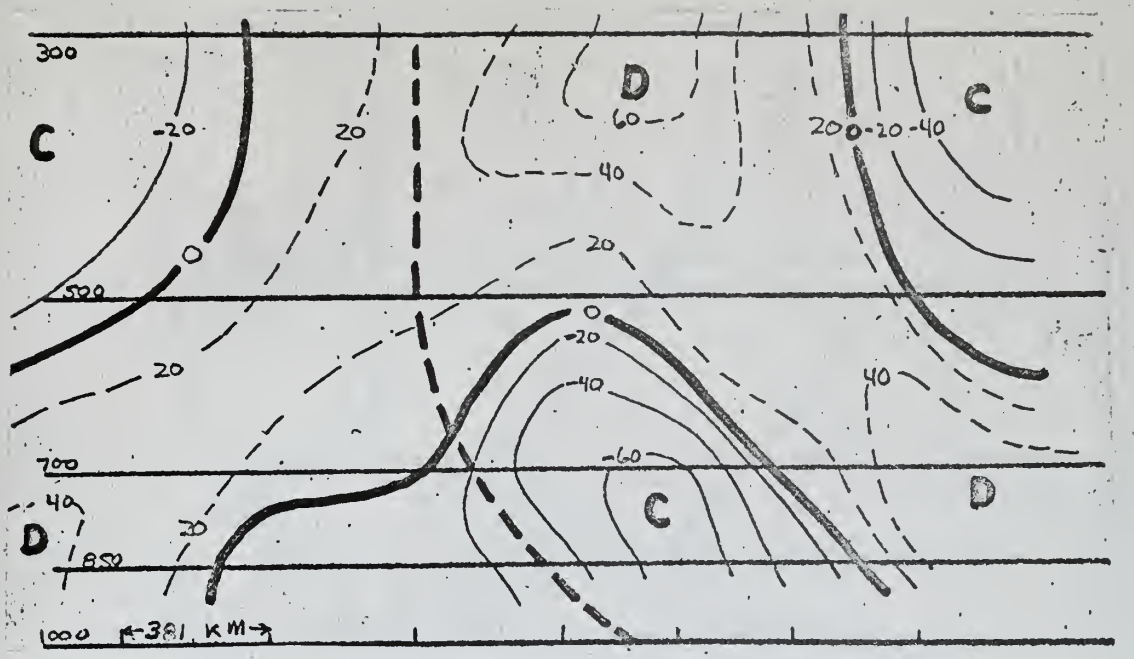

Figure 16a. Cross section of divergence in units of 10^{-7} per second taken along line AA' on figure 8a. (12Z 17 March)

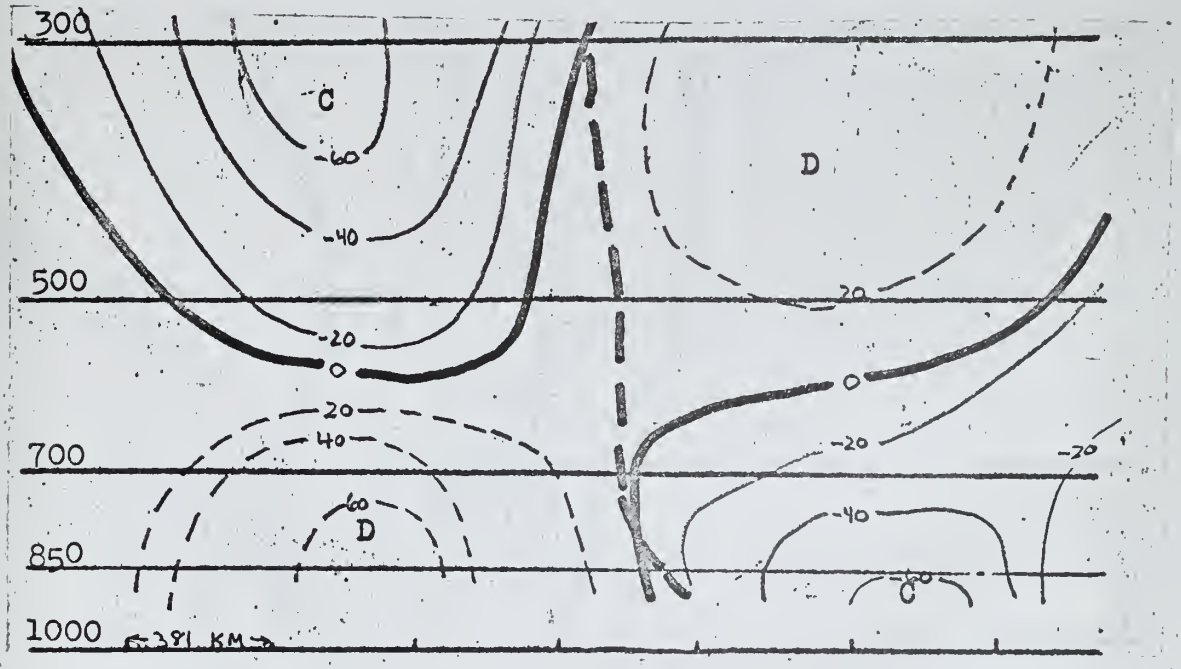

Figure 16b. Cross section of divergence in units of 10^{-7} per second taken along line AA' on figure 9a. (00Z 18 March)

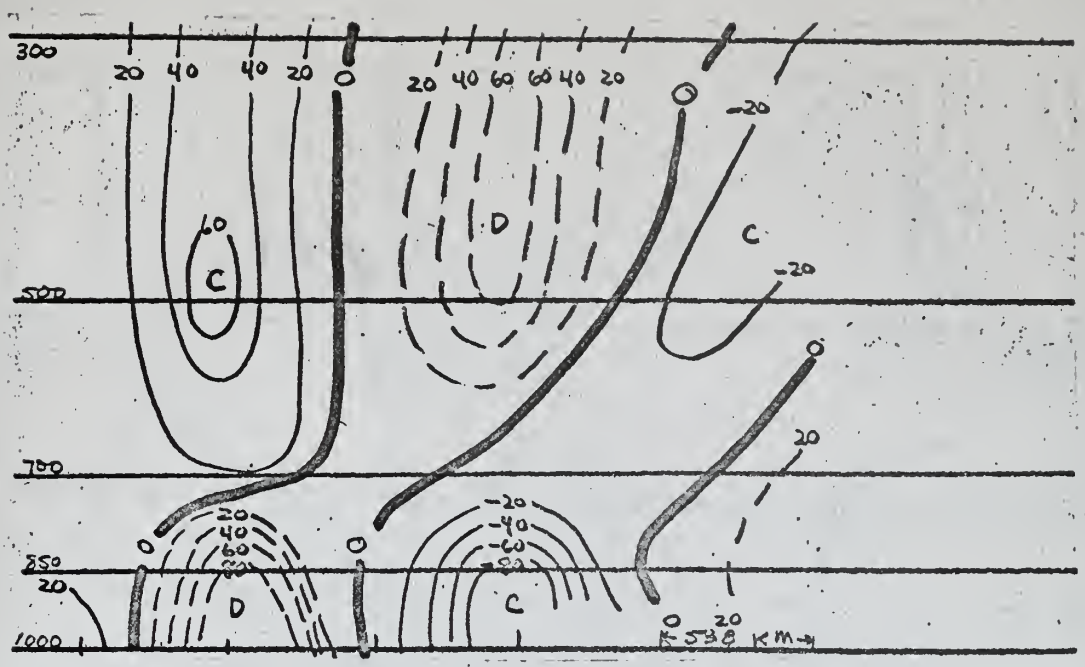

Figure 17a. Cross section of divergence in units of 10^{-7} per second taken along line BB' on figure 9b. (00Z 18 March)

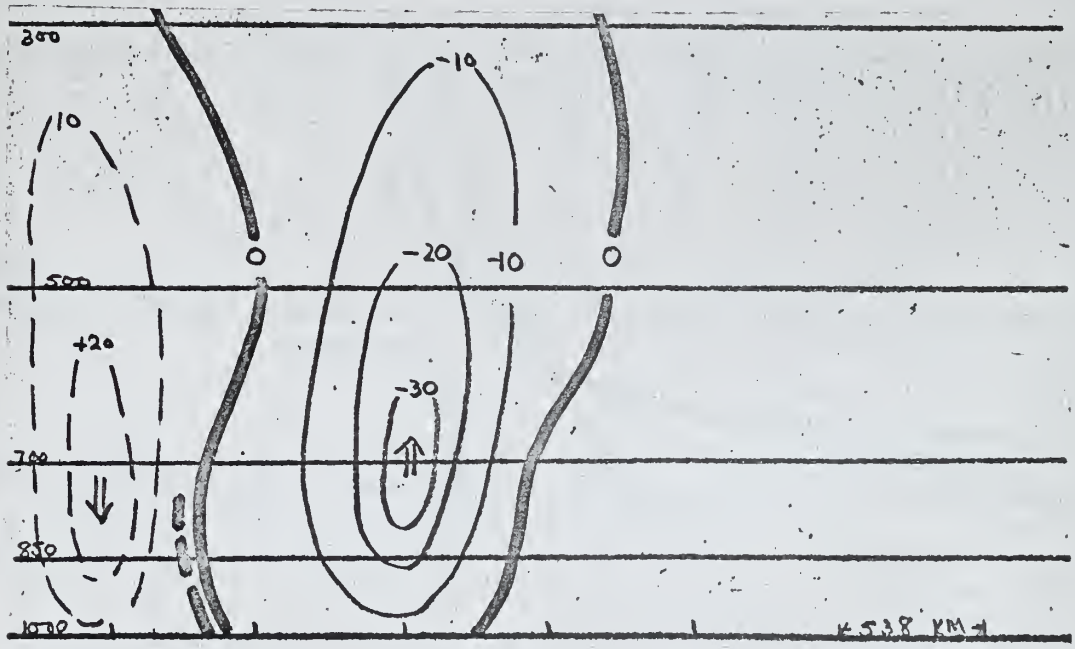

Figure 17b. Cross section of vertical velocity in units of 10^{-4} mb per second taken along line BB'on figure 9b. (00Z 18 March)

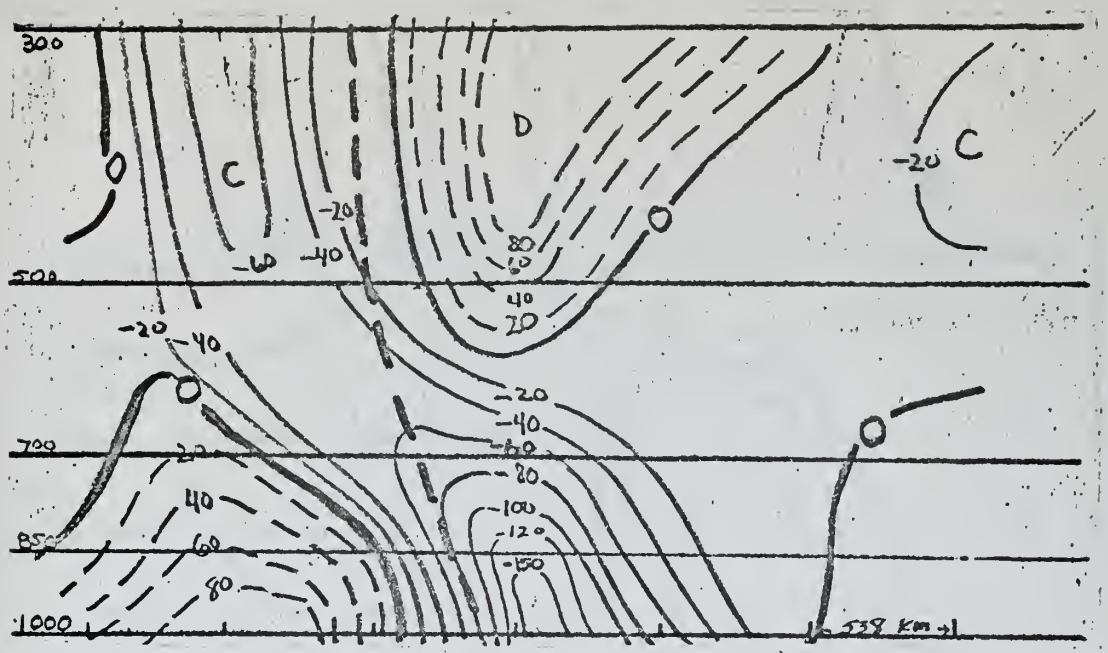

Figure 18a. Cross section of divergence in units of 10^{-7} per second taken along line AA' on figure 10a. (12Z 18 March)

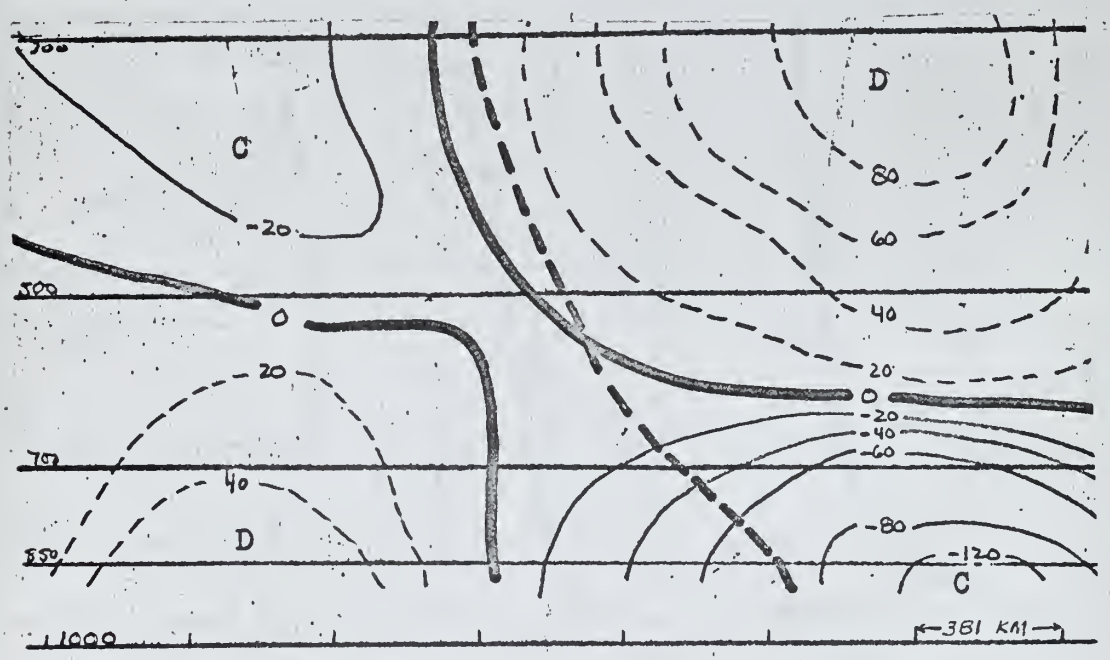

Figure 18b. Cross section of divergence in units of 10^{-7} per second taken along line AA' on figure 12a. (00Z 19 March)

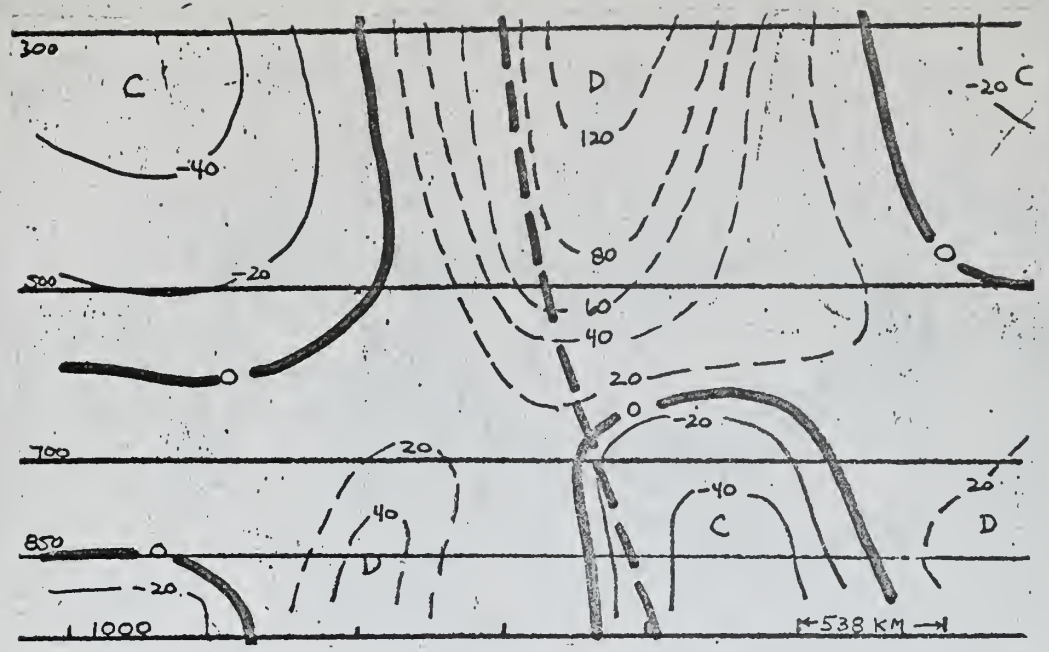

Figure 19a. Cross section of divergence in units of 10^{-7} per second taken along line AA' on figure 13a. (12Z 19 March)

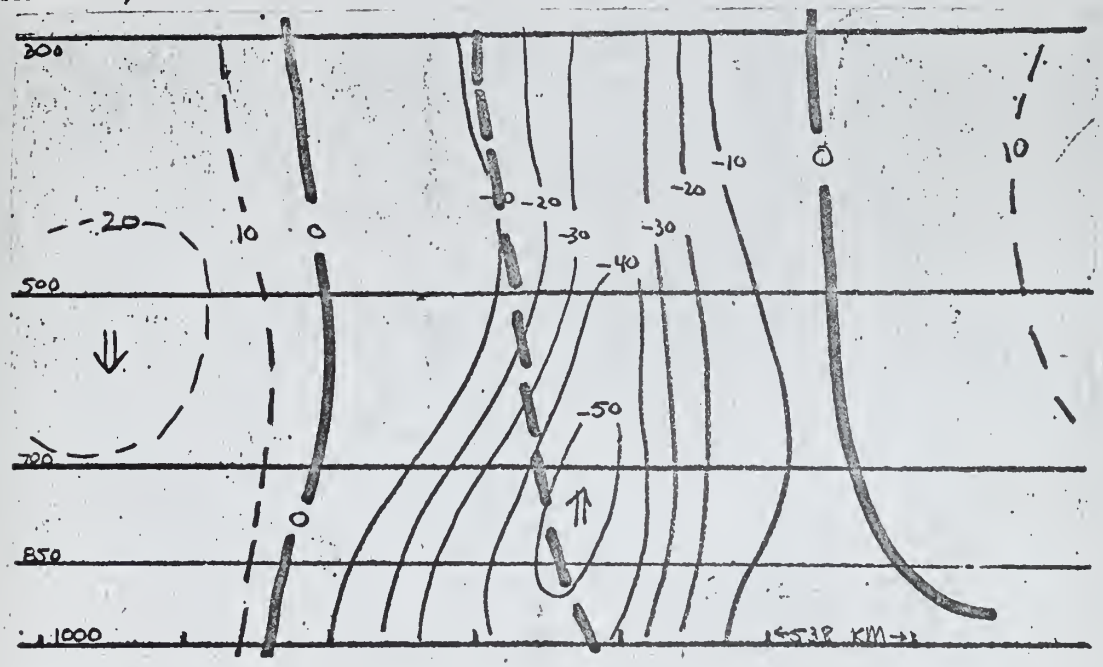

Figure 19b. Cross section of vertical velocity in units of 10^{-4} mb per second taken along line AA' on figure 13a. (12Z 19 March)

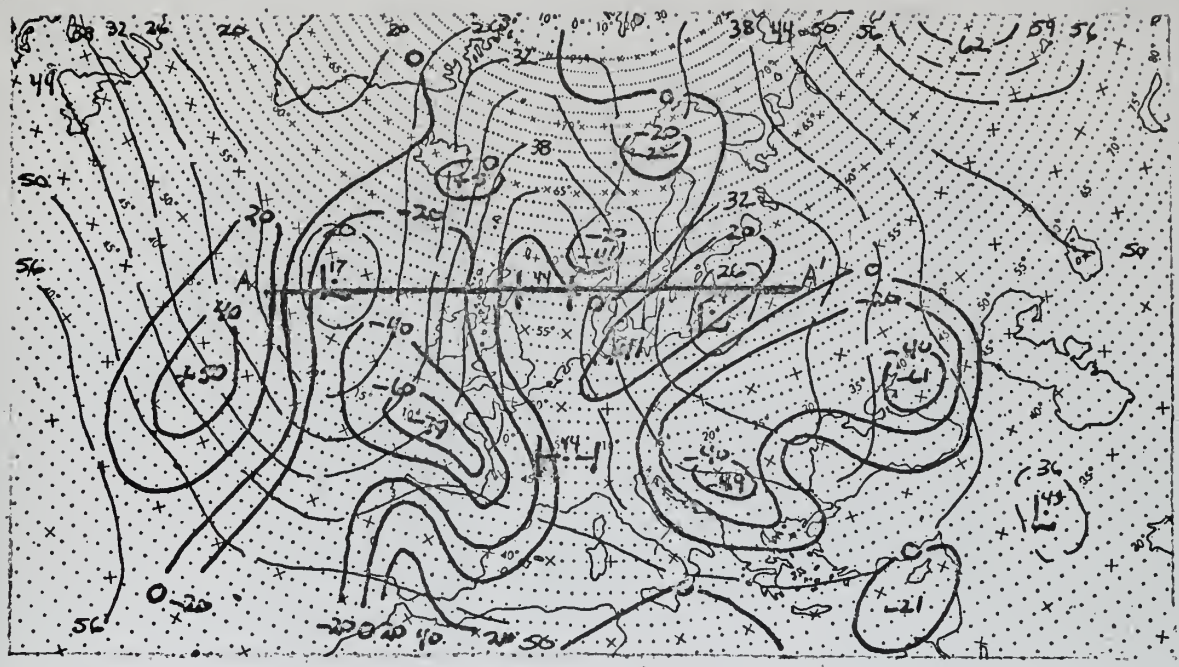

Figure 20a. 850-mb divergence in units of 10^{-7} per second and 850-mb height analysis (50~1,500 meters) at 00Z 13 February 1964.

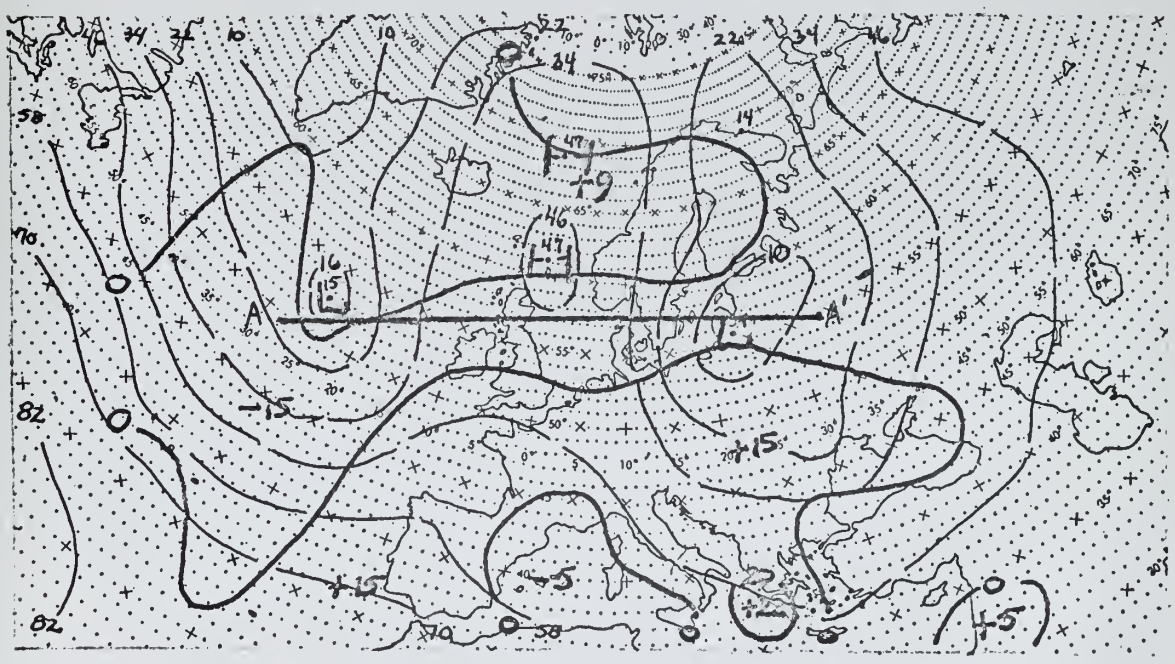

Figure 20b. 500-mb divergence in units of 10^{-7} per second and 500-mb analysis (22~5,220 meters) at 00Z 13 February 1964.

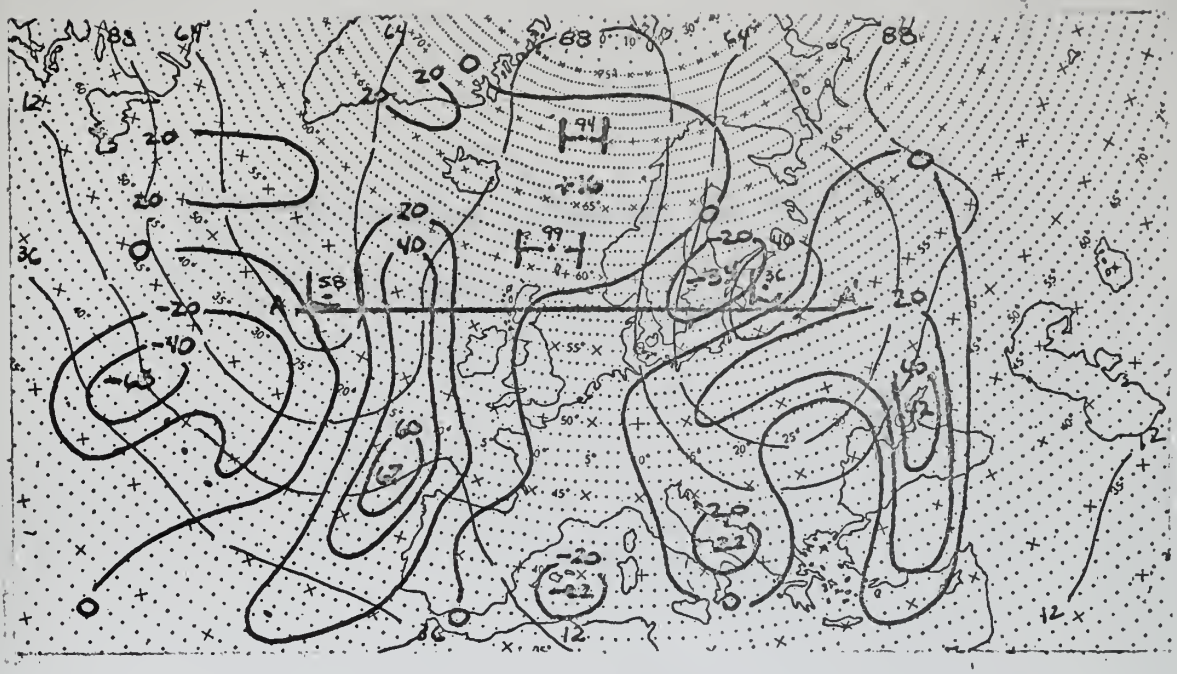

Figure 21a. 300-mb divergence in units of 10^{-7} per second and 300-mb height analysis (12 ~ 9,120 meters) at 00Z 13 February 1964.

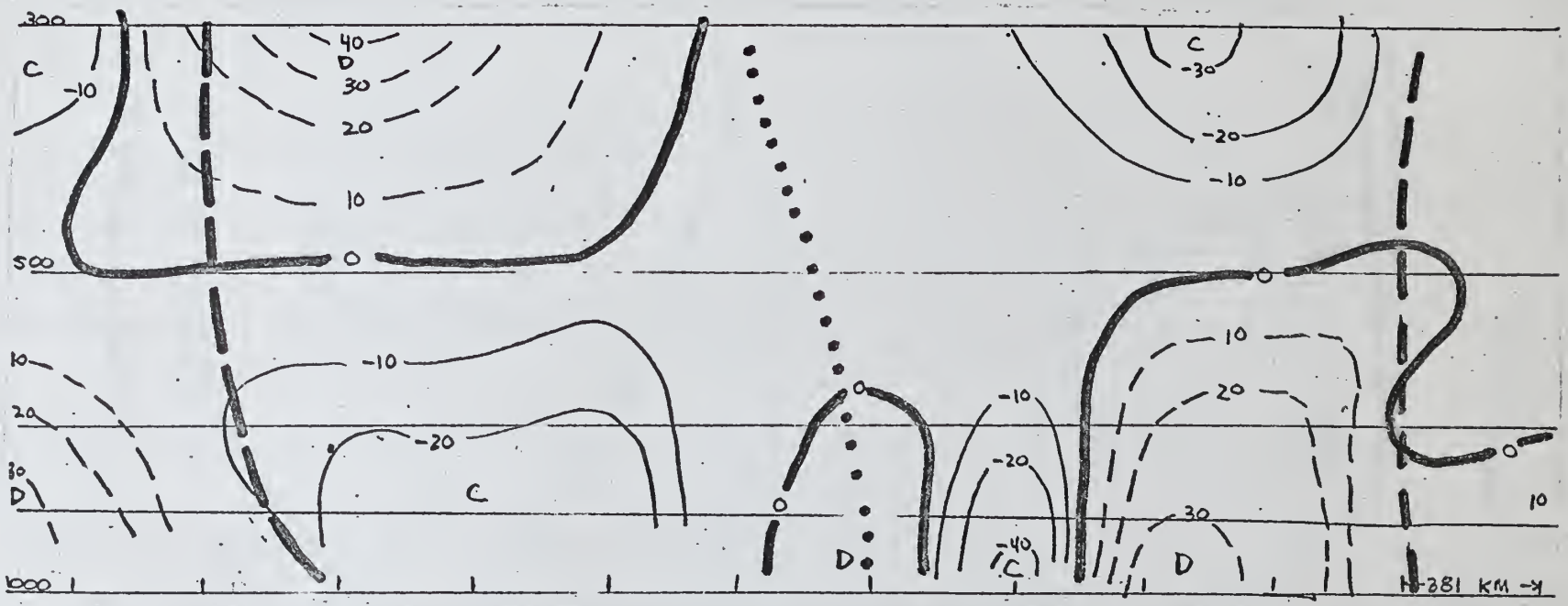

Figure 22. Cross section of divergence in units of 10^{-7} per second taken along line AA' on figure 20a. (00Z 13 February)

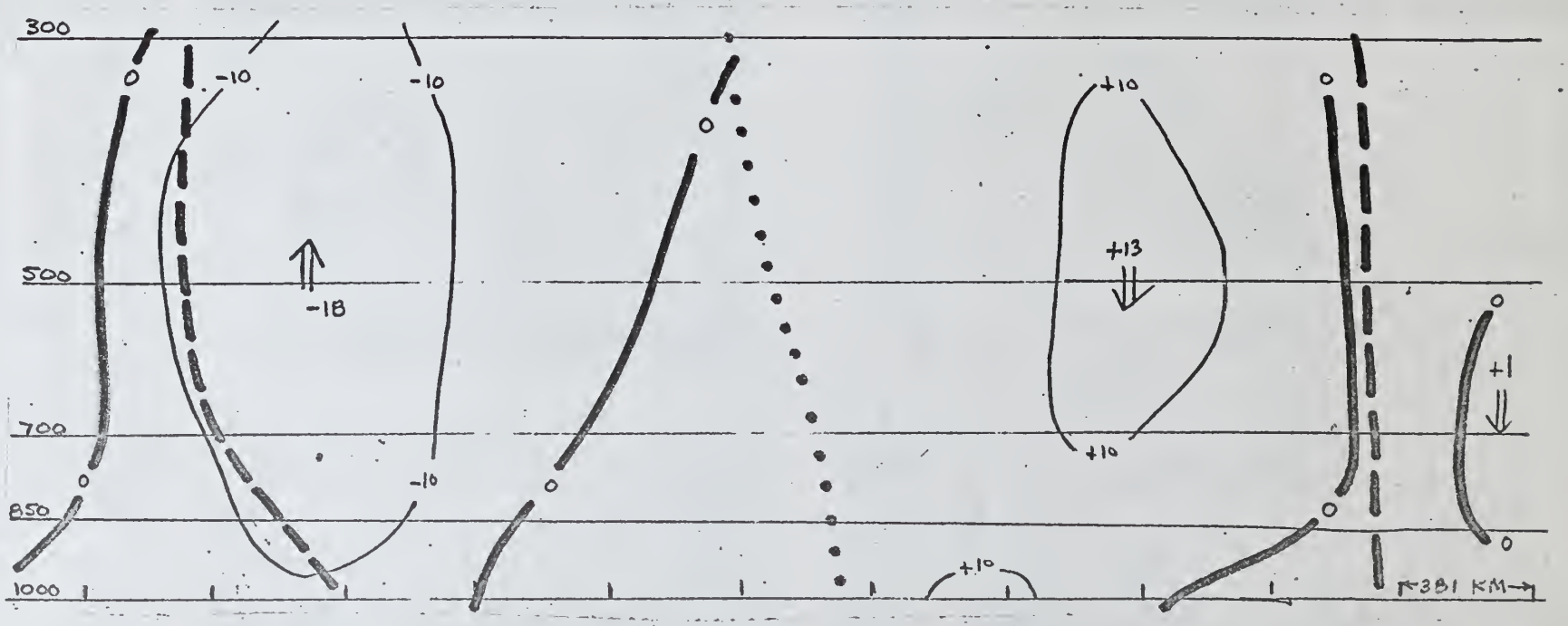

Figure 23. Cross section of vertical velocity in units of 10^{-4} mb per second taken along line AA' on figure 20a. (00Z 13 February)

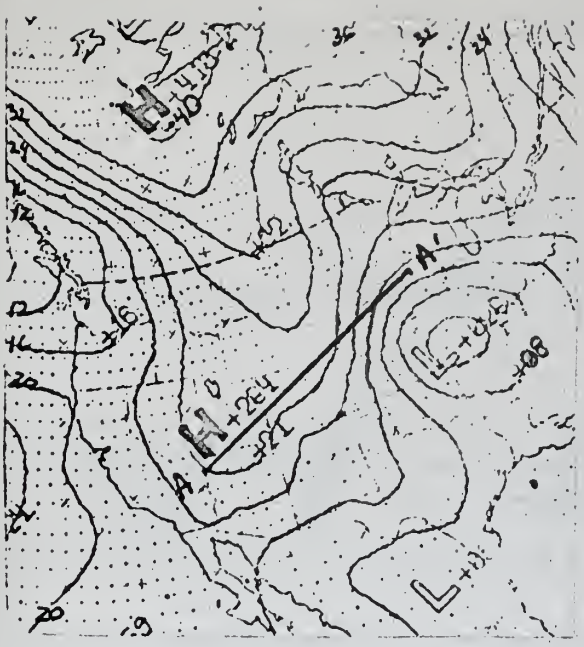

Figure 24a. Surface analysis at 12Z 20 March 1964. (32 ~ 1032 mb)

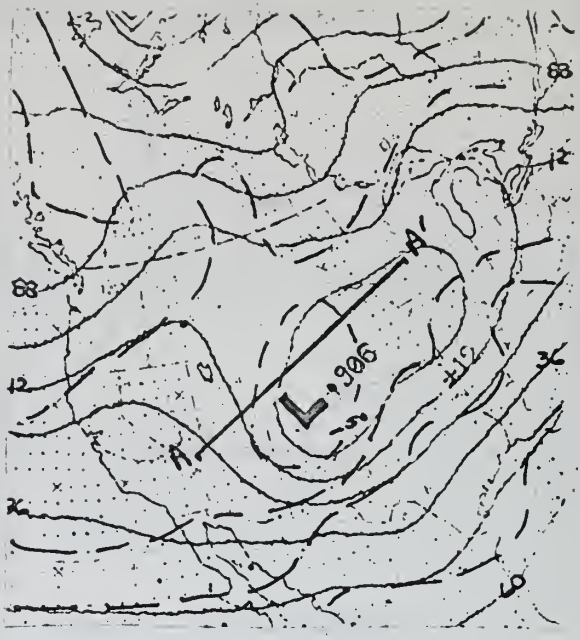

Figure 24b. 300-mb height analysis (12 ~ 9,120 meters) at 12Z 20 March 1964.

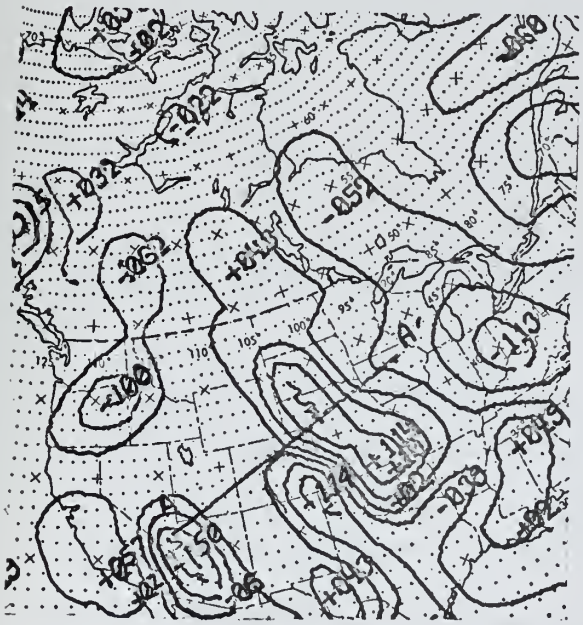

Figure 24c. 850-mb divergence in units of 10^{-7} per second at 12Z 20 March 1964.

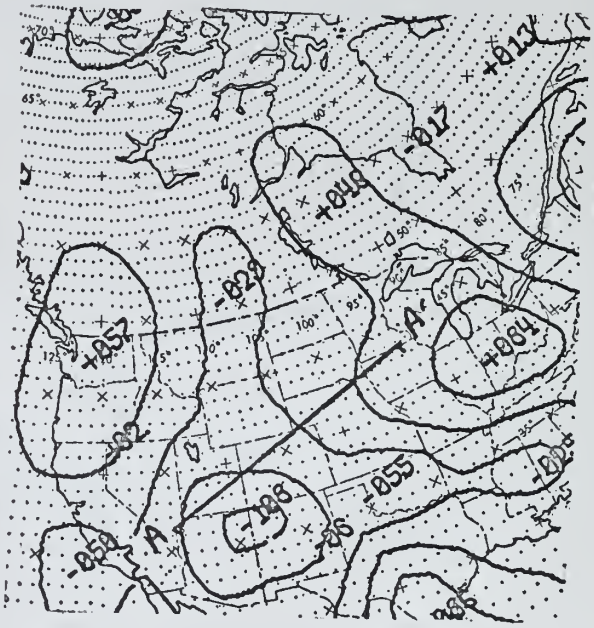

Figure 24d. 300-mb divergence in units of 10^{-7} per second at 12Z 20 March 1964

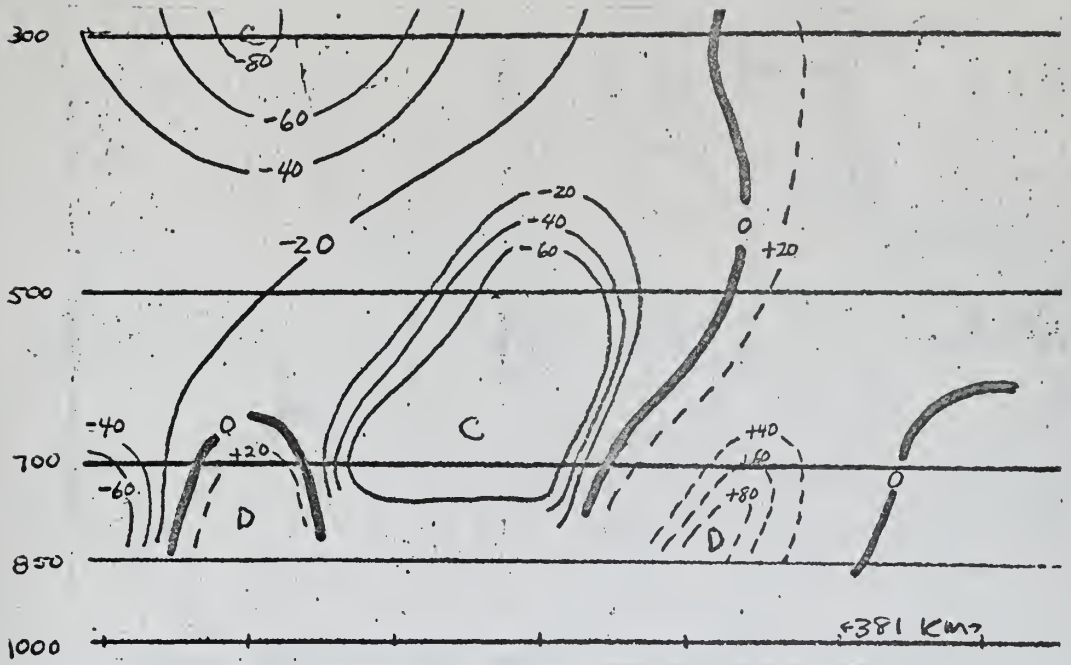

Figure 25a. Cross section of divergence in units of 10^{-7} per second taken along line AA' on figure 24. (12Z 20 March)

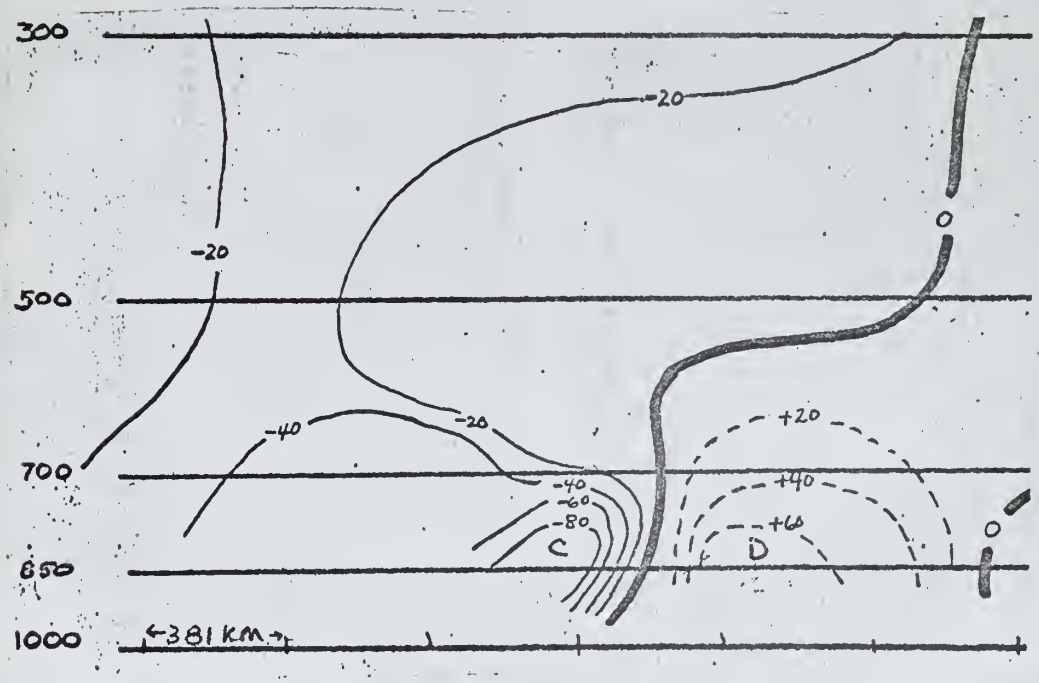

Figure 25b. Cross section of divergence in units of 10^{-7} per second taken along line AA' on fig. 26. (00Z 21 March)

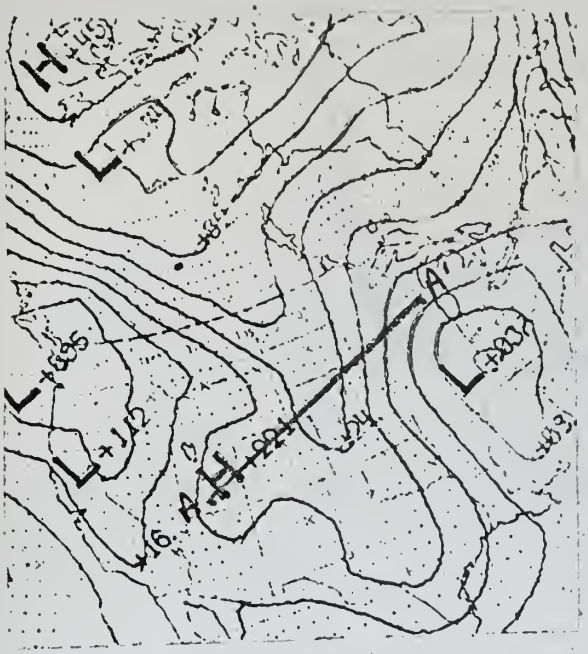

Figure 26a. Surface analysis at 00Z 21 March 1964. (32 ~ 1032 mb)

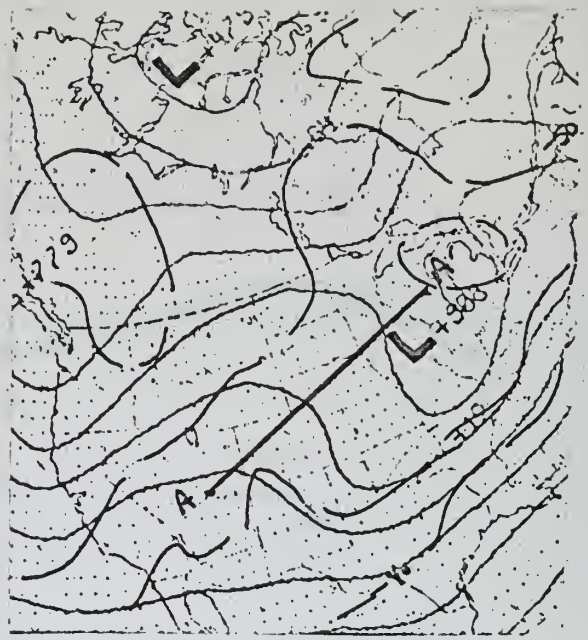

Figure 26b. 300-mb analysis (12 ~ 9,120 meters) at 00Z 21 March 1964.

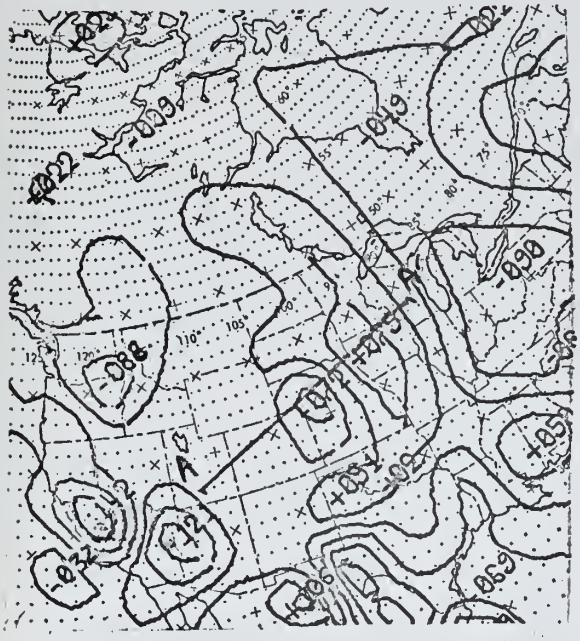

Figure 26c. 850-mb divergence in units of 10^{-7} per second at 00Z 21 March 1964.

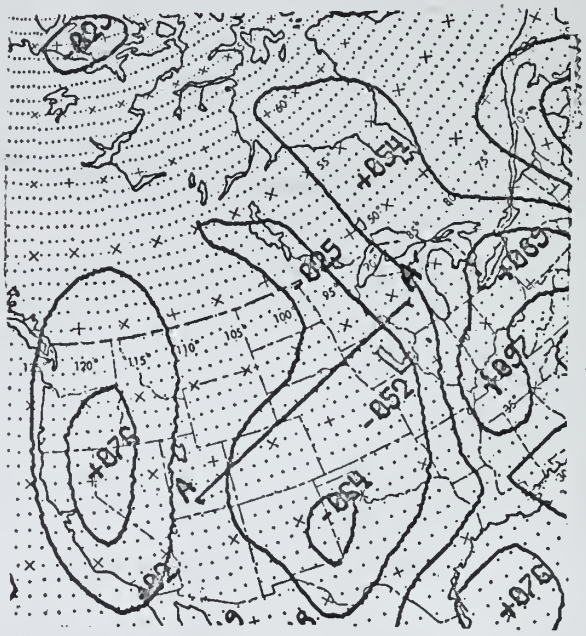

Figure 26d. 300-mb divergence in units of 10^{-7} per second at 00Z 21 March 1964.

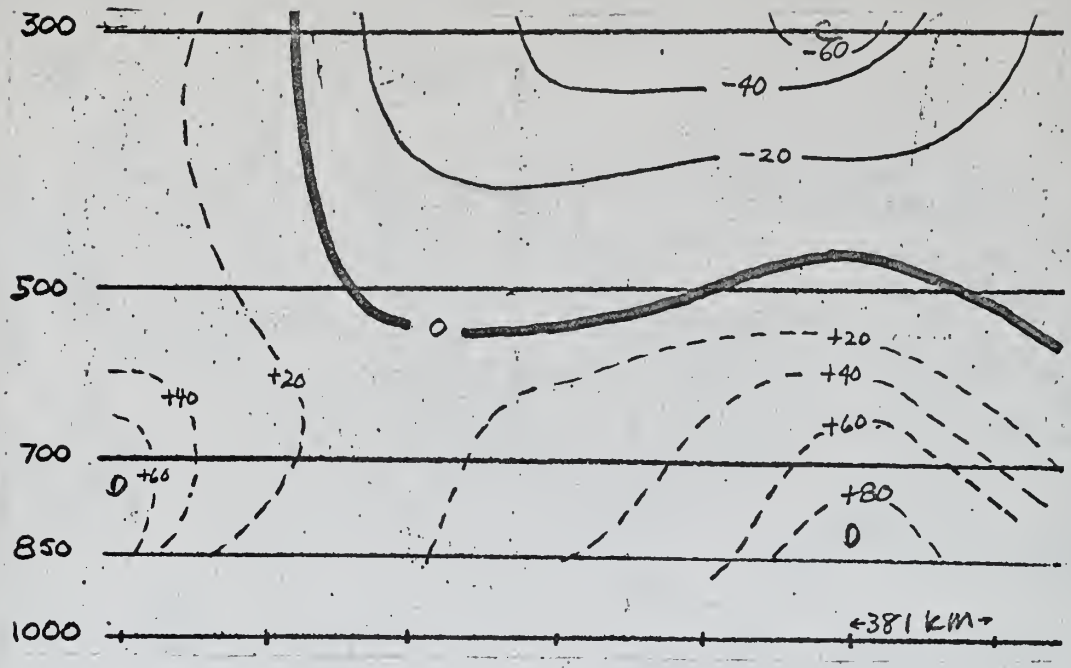

Figure 27a. Cross section of divergence in units of 10^{-7} per second taken along line AA' on figure 28.

(00Z 22 March)

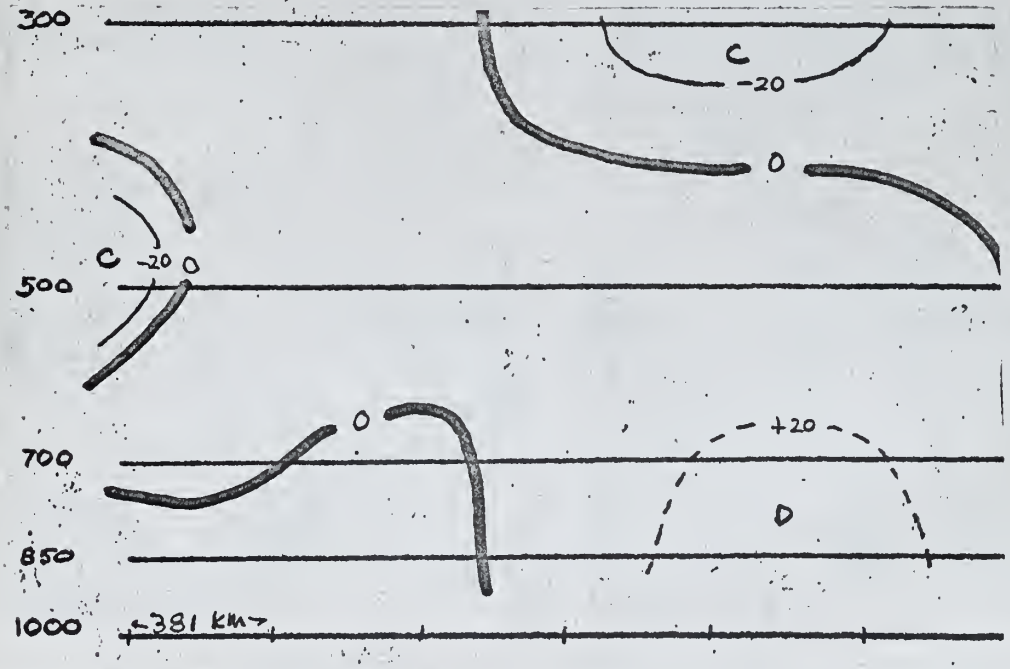

Figure 27 b . Cross section of divergence in units of 10^{-7} per second taken along line AA' on figure 29.

(. 12Z 22 March)

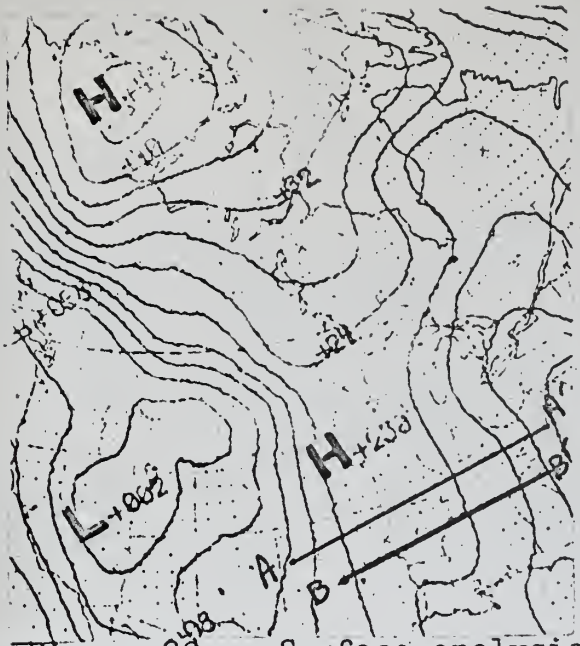

Figure 28a. Surface analysis at 00Z 22 March 1964. (32 ~ 1032 mb)

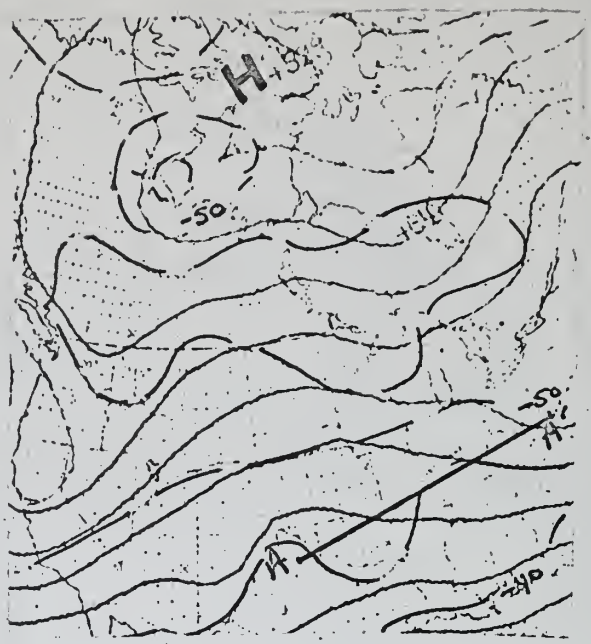

Figure 28b. 300-mb analysis (12 ~ 9,120 meters) at 00Z 22 March 1964.

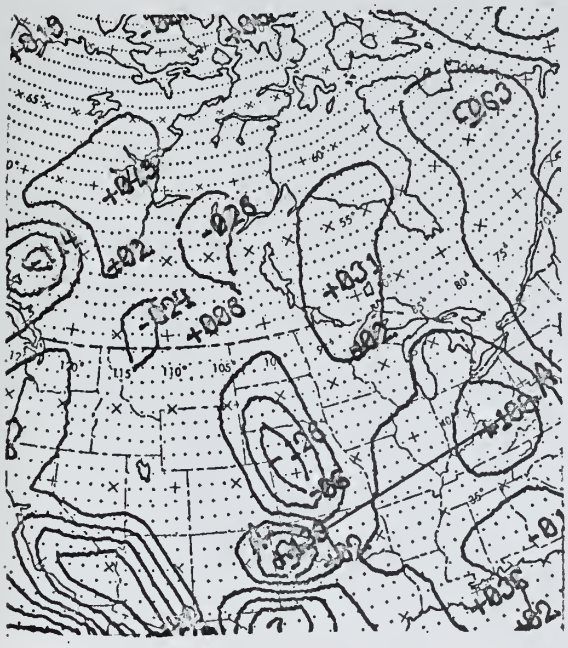

Figure 28c. 850-mb divergence in units of 10^{-7} per second at 00Z 22 March 1964.

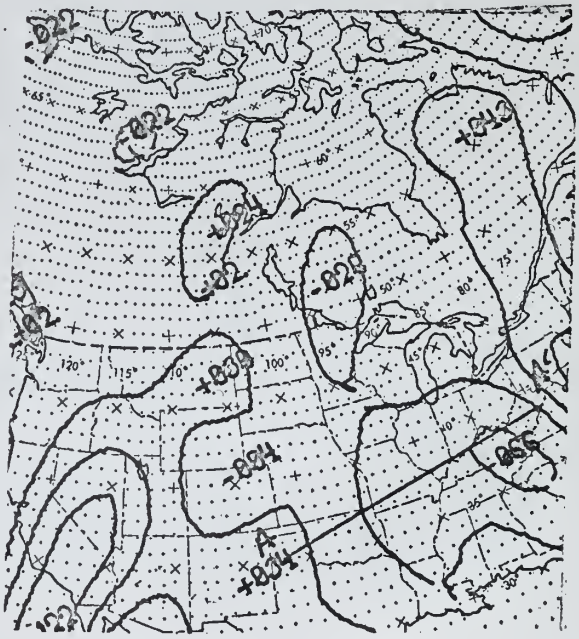

Figure 28d. 300-mb divergence in units of 10^{-7} per second at 00Z 22 March 1964.

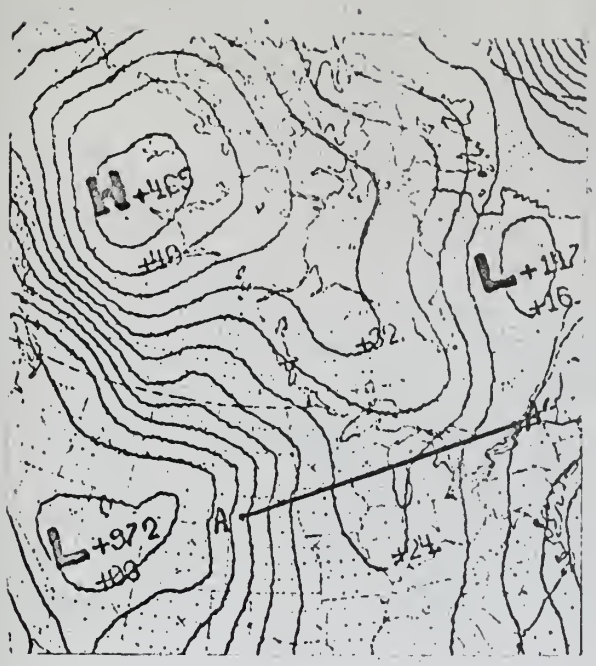

Figure 29a. Surface analysis at 12Z 22 March 1964. (32~1032 mb)

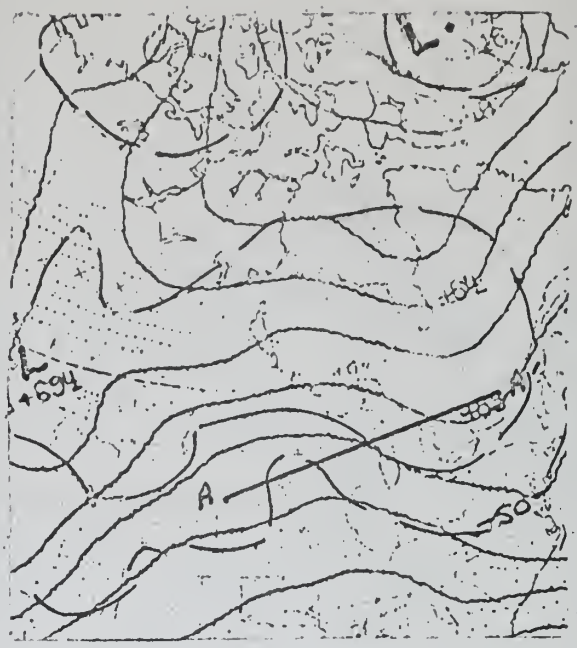

Figure 29b. 300-mb analysis (12~9,120 meters) at 12Z 22 March 1964.

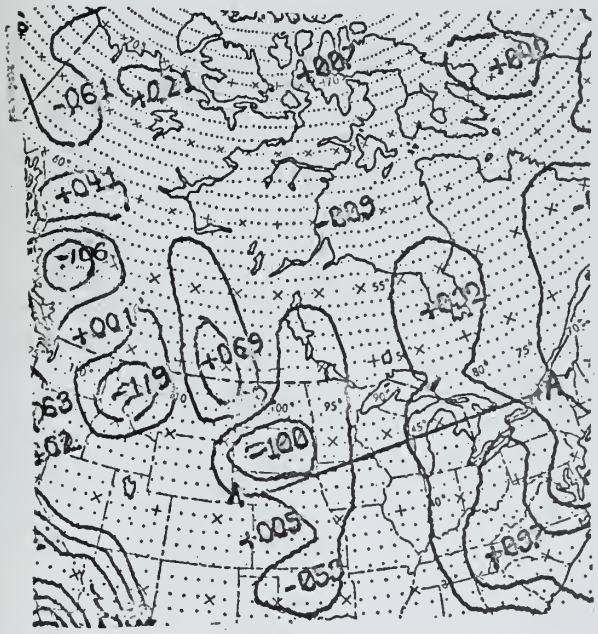

Figure 29c. 850-mb divergence in units of 10^{-7} per second at 12Z 22 March 1964.

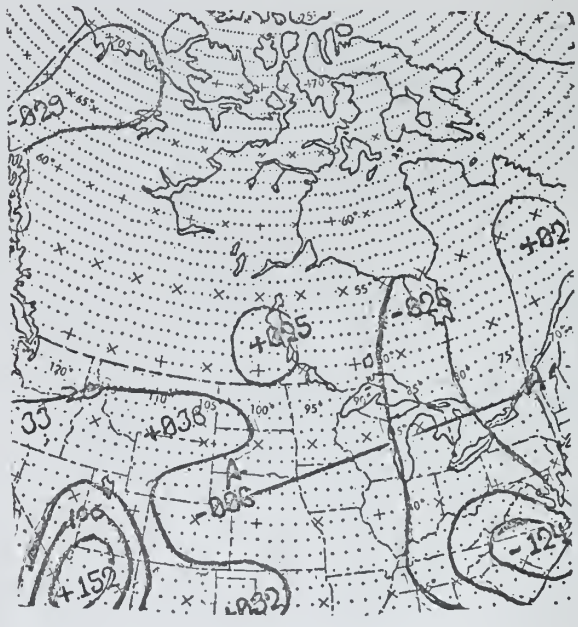

Figure 29d. 300-mb divergence in units of 10^{-7} per second at 12Z 22 March 1964.

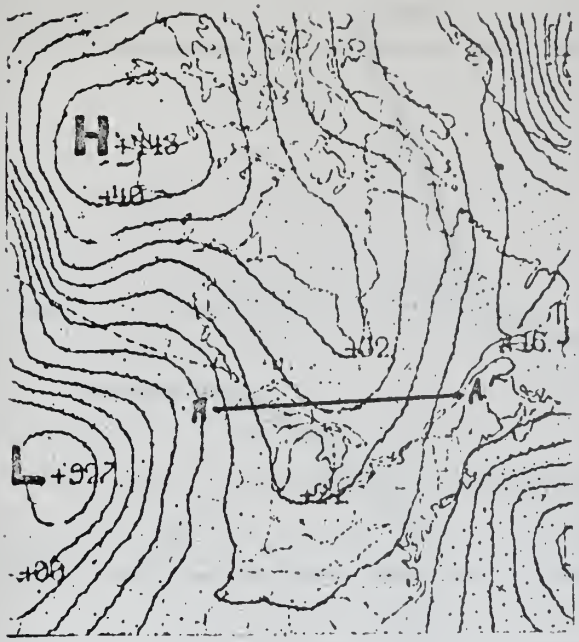

Figure 30a. Surface analysis at 00Z 23 March 1964. (32 ~ 1032 mb)

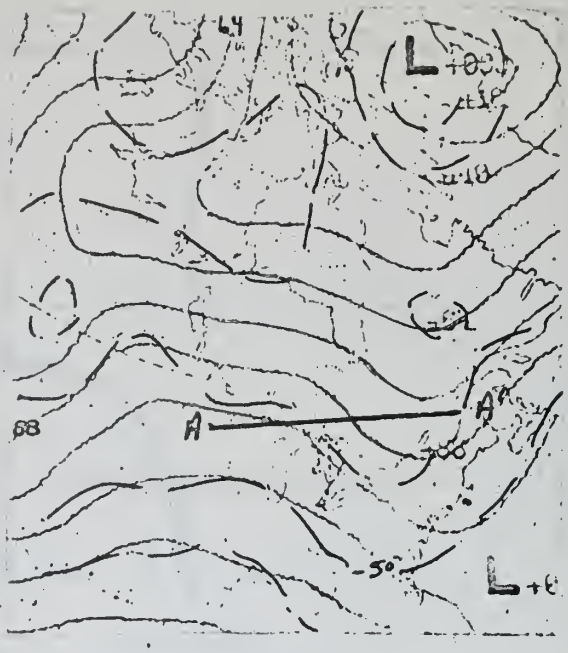

Figure 30b. 300-mb analysis (12 ~ 9,120 meters) at 00Z 23 March 1964.

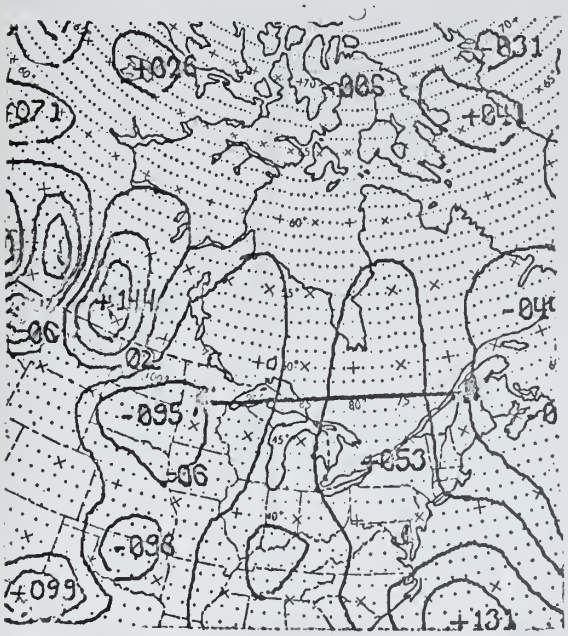

Figure 30c. 850-mb divergence in units of 10^{-7} per second at 00Z 23 March 1964.

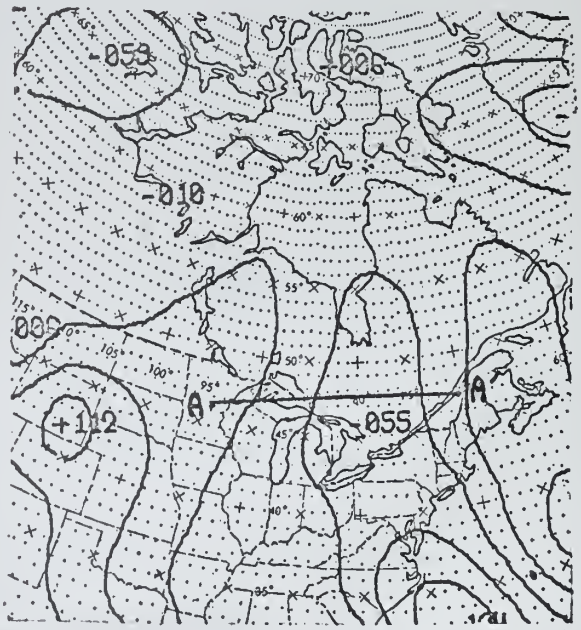

Figure 30b. 300-mb divergence in units of 10^{-7} per second at 00Z 23 March 1964.

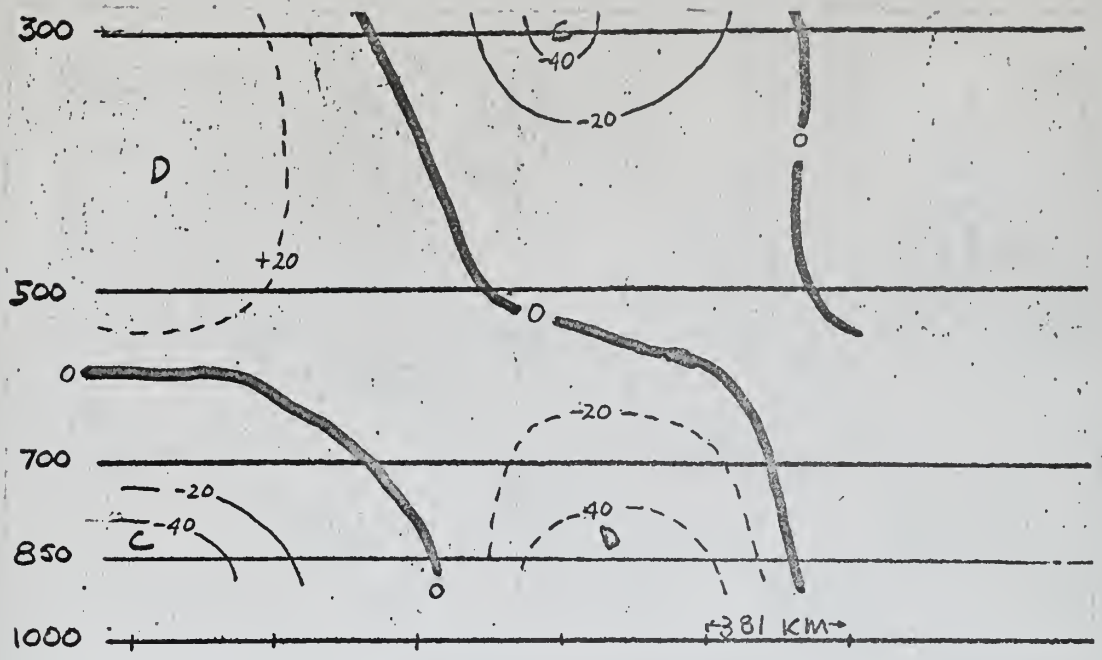

Figure 31a. Cross section of divergence in units of 10^{-7} per second taken along line AA' on figure 30. (00Z 23 March)

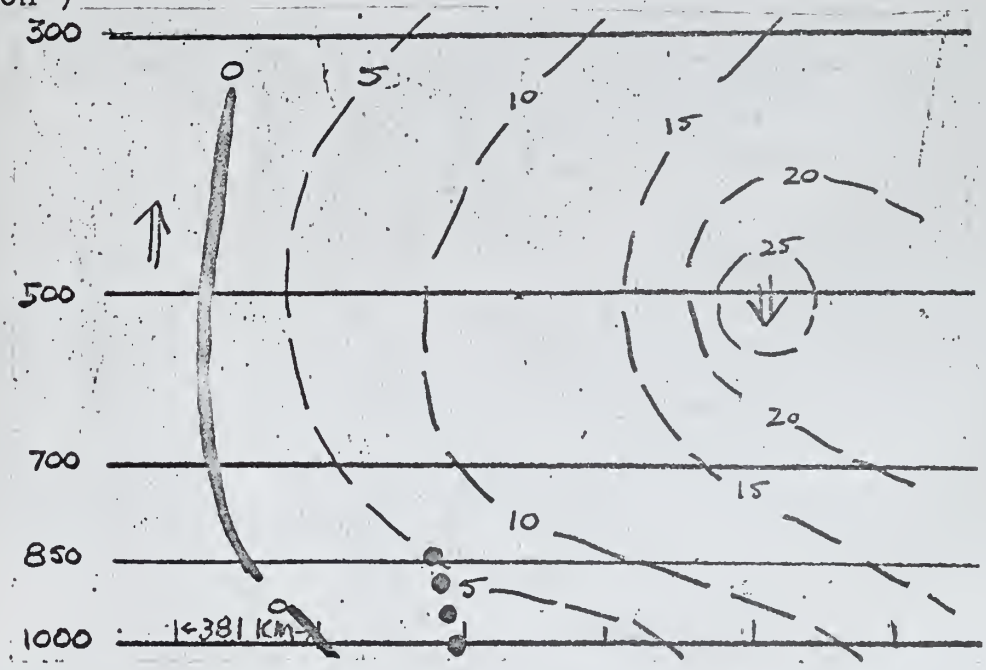

Figure 31b. Cross section of vertical velocity in units of 10^{-4} mb per second taken along line BB' on figure 28a. (00Z 22 March)

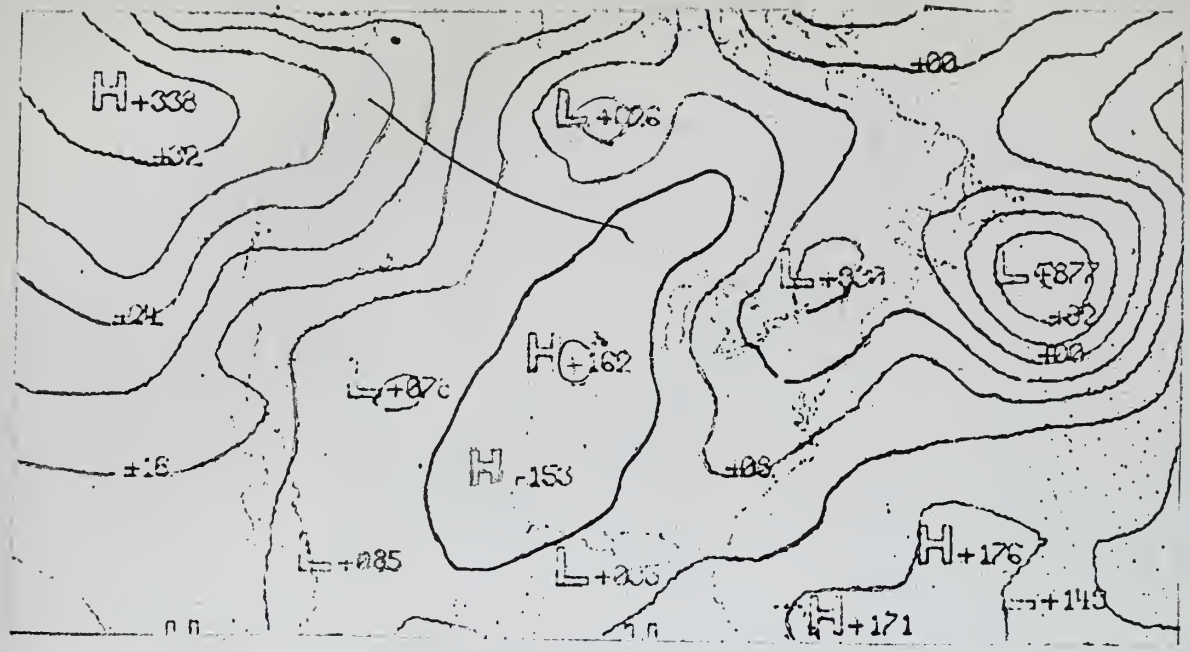

Figure 32a. Surface pressure analysis at 00Z 14 February 1964. (32~1032 mb)

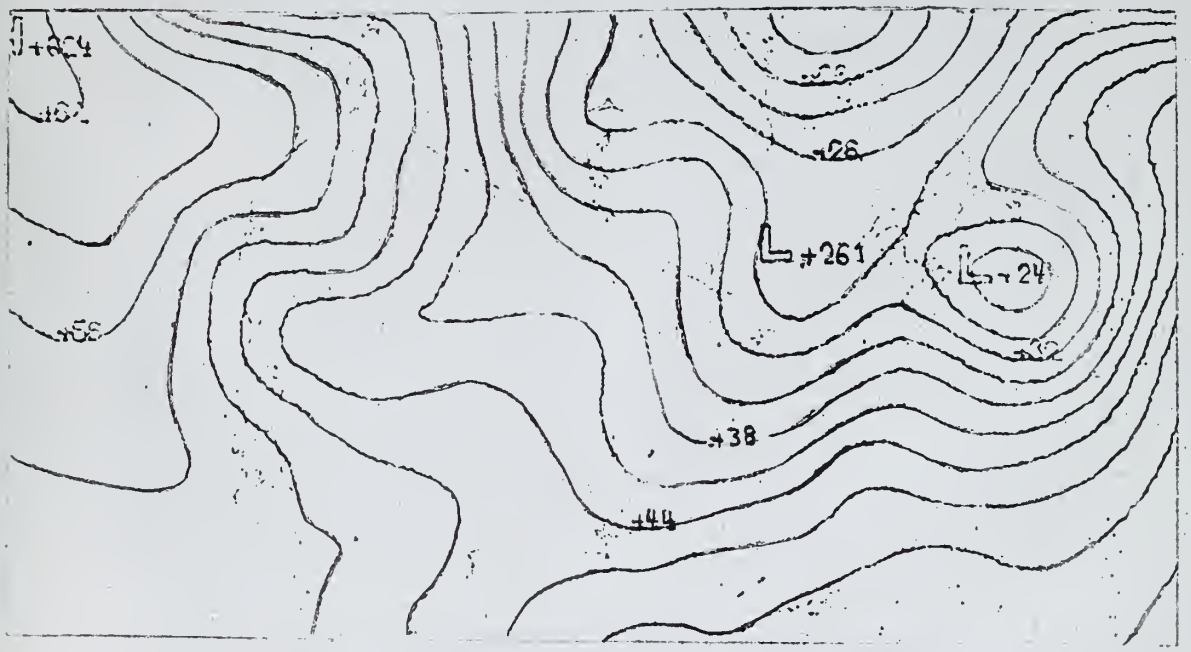

Figure 32b. 850-mb height analysis (50~1,500 meters) at 00Z 14 February 1964.

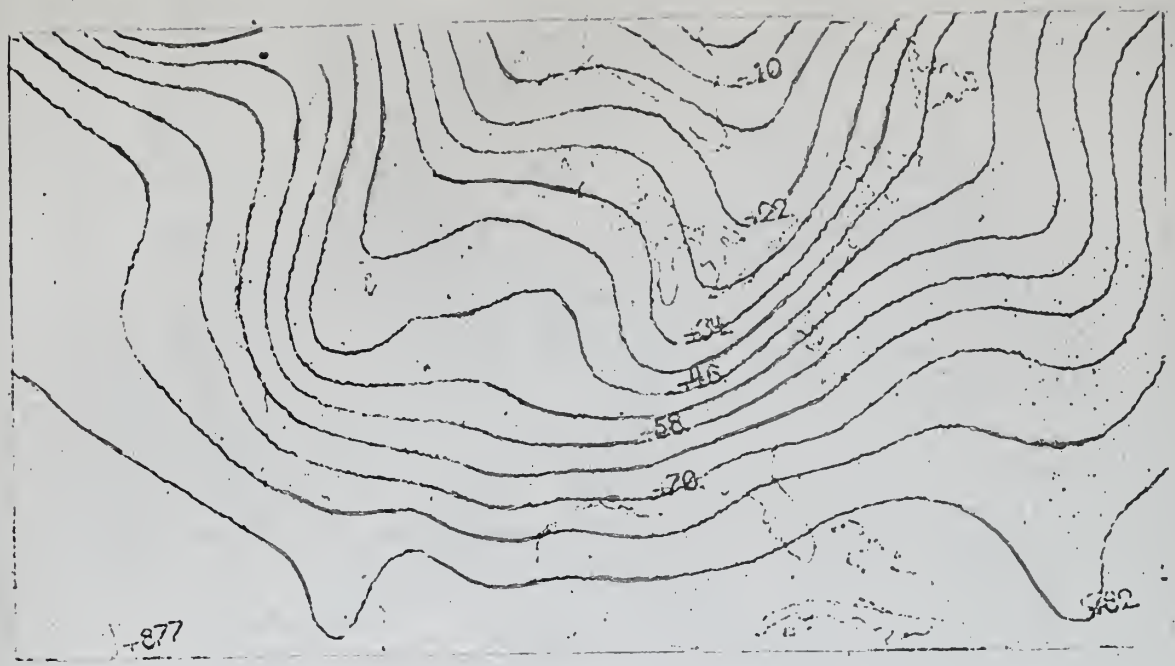

Figure 33a. 500-mb height analysis (22 ~ 5,220 meters) at 00Z 14 February 1964.

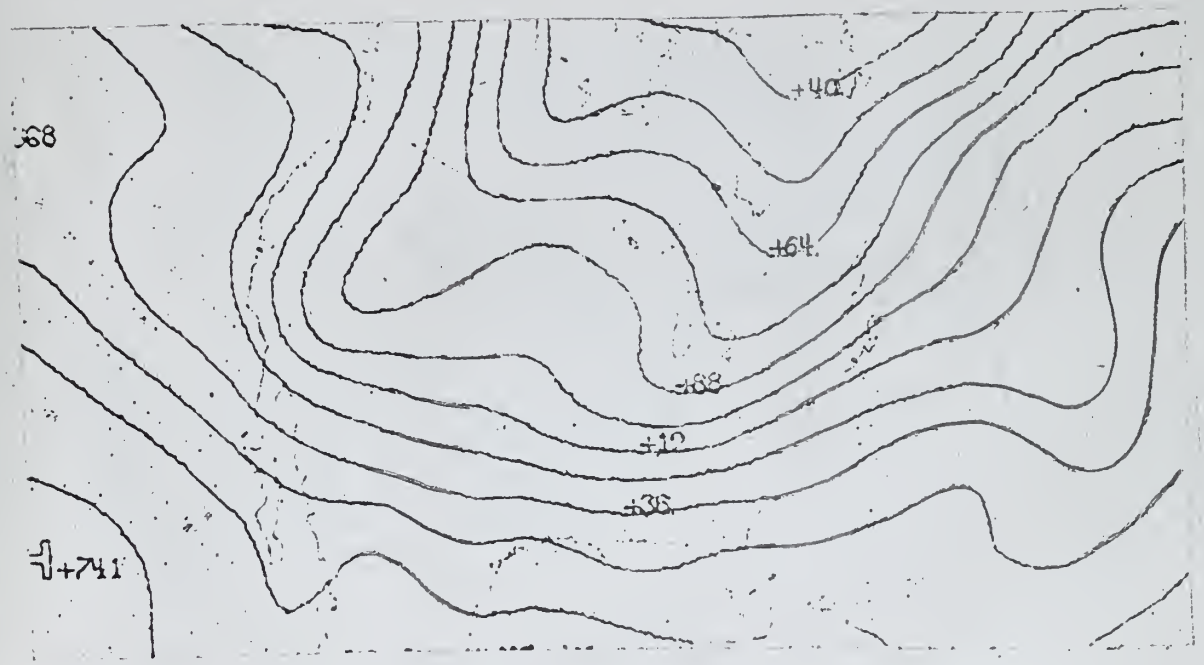

Figure 33b. 300-mb height analysis (12 ~ 9,120 meters) at 00Z 14 February 1964.

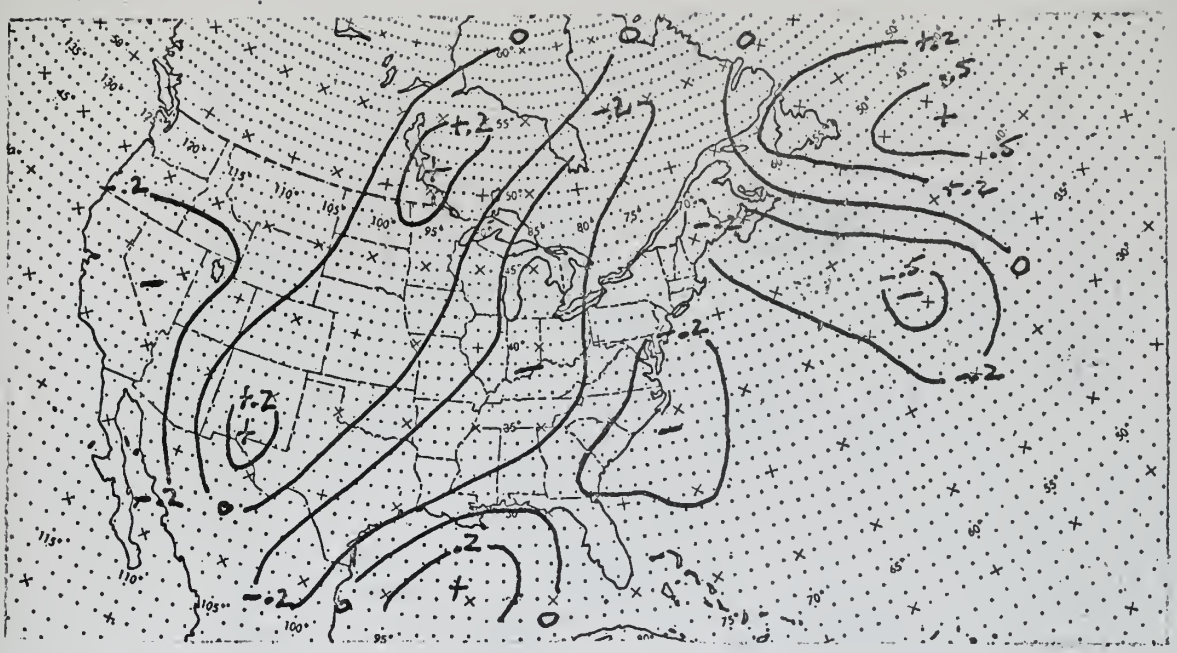

Figure 34a. 850-mb thermal advection with the non-divergent wind in degrees Centigrade per hour at 00Z 14 February 1964.

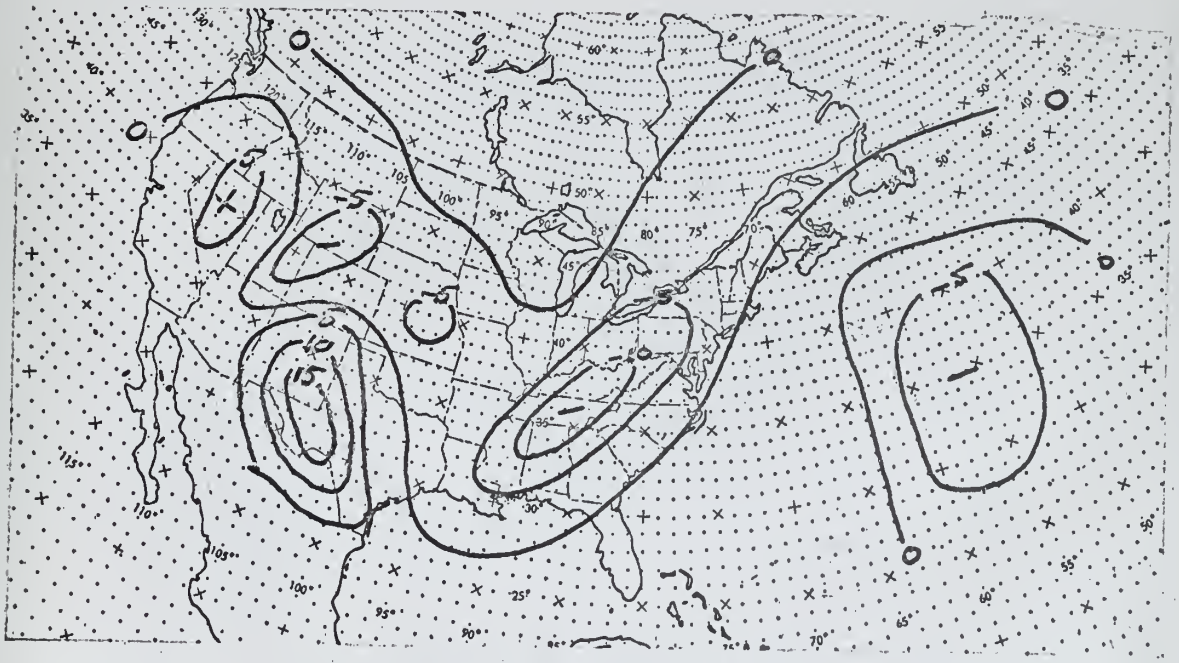

Figure 34b. 850-mb thermal advection with the divergent wind in degrees Centigrade per hour x 10^{-5} at 00Z 14 February 1964.

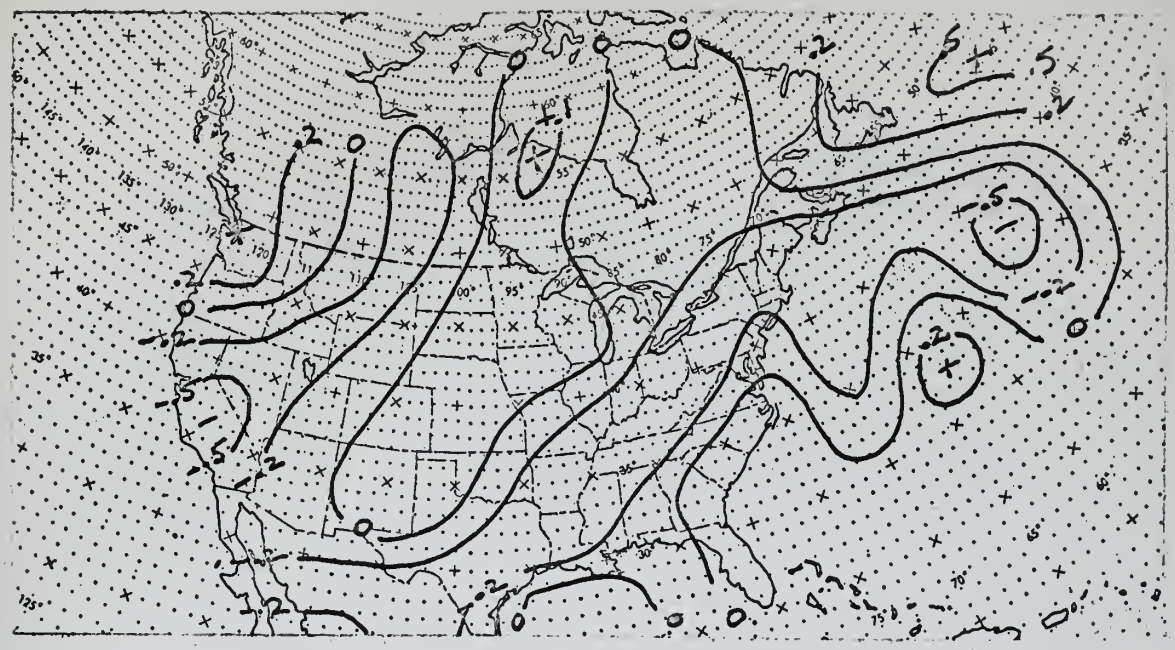

Figure 35a. 700-mb thermal advection with the non-divergent wind in degrees Centigrade per hour at 00Z 14 February 1964.

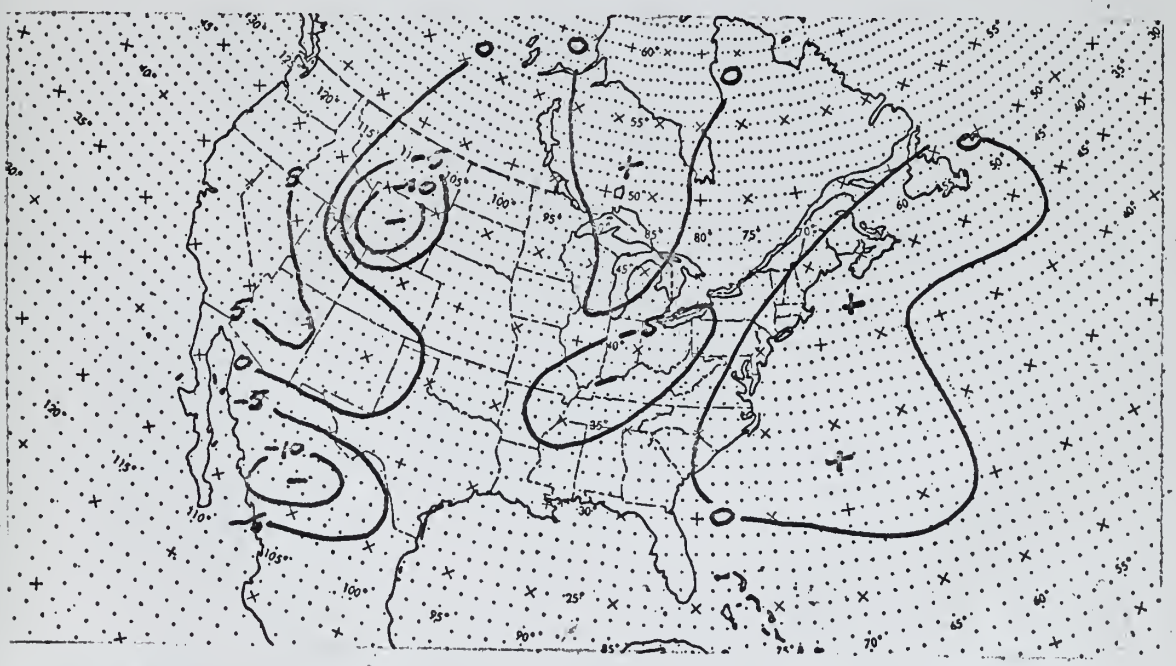

Figure 35b. 700-mb thermal advection with the divergent wind in degrees Centigrade per hour x 10^2 at 00Z 14 February 1964.

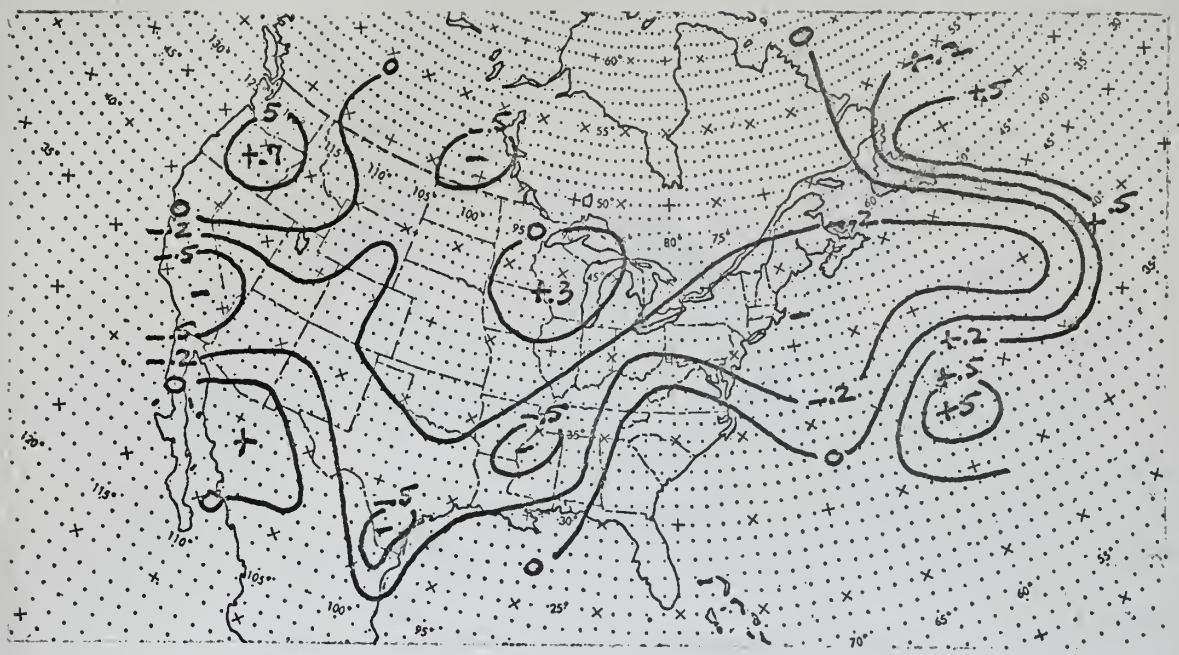

Figure 36a. 500-mb thermal advection with the non-divergent wind in degrees Centigrade per hour at 00Z 14 February 1964.

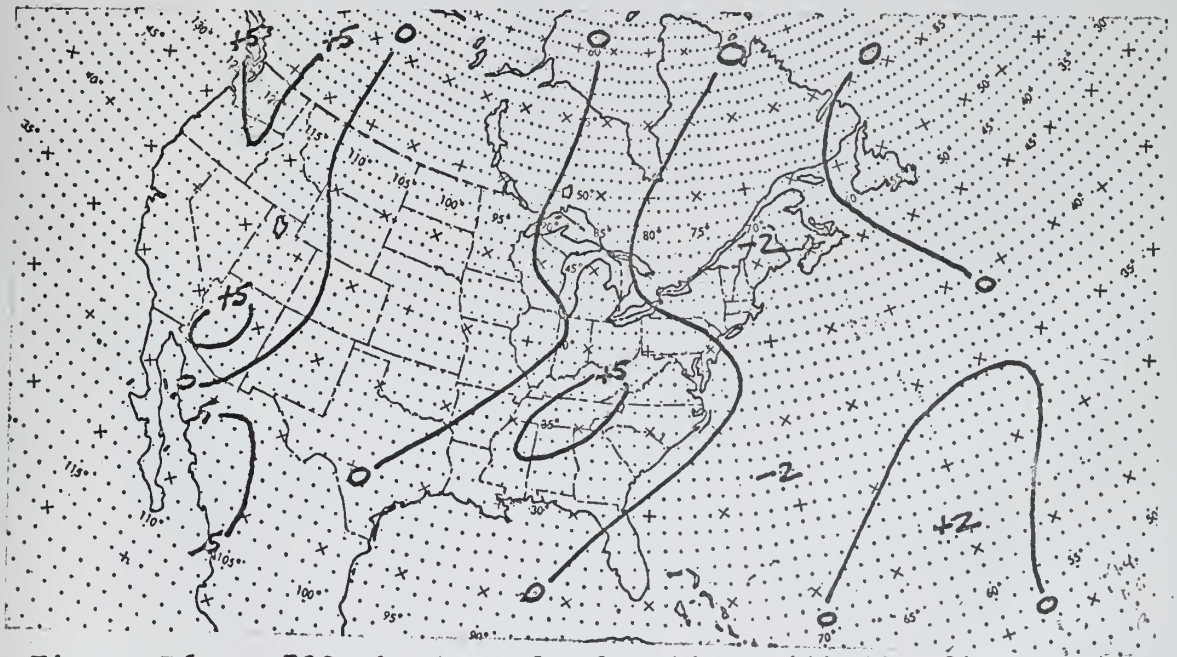

Figure 36b. 500-mb thermal advection with the divergent wind in degrees Centigrade per hour x 10^2 at 00Z 14 February 1964.

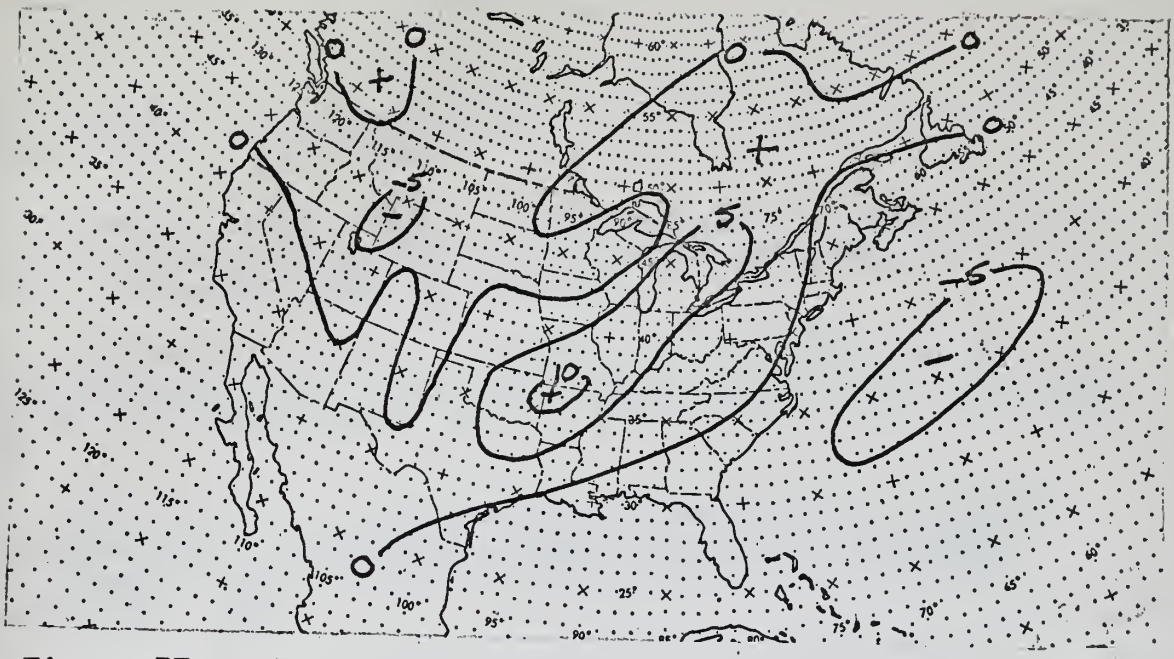

Figure 37 . 300-mb thermal advection with the divergent wind in degrees Centigrade per hour x 10^{-2} at 00Z 14 February 1964.

BIBLIOGRAPHY

1. Cressman, G. P. A diagnostic study of mid-tropospheric development. Monthly Weather Review, vol. 89, No. 3, March, 1961, pp. 74-82.

2. Fleagle, R. F. Quantitative analysis of factors influencing pressure change. Journal of Meteorology, vol. 5, No. 6, December, 1948, pp. 281-292.

3. Haltiner, G. J., L. C. Clarke, G. E. Lawniczak Jr. Computation of the large scale vertical velocity. Journal of Applied Meteorology, vol. 2, No. 2, April, 1963, pp. 242-259.

4. Lacey, F. E. A comparison of numerically determined divergent and non-divergent winds to geostropic winds, M.S. thesis, U. S. Naval Postgraduate School, Monterey, California, 1962.

5. Stuart, D. W. Vertical motion and the baroclinic mechanism of rapid upper level cyclogenesis. University of California, Los Angeles, California, December 1961.

thesA34
The distribution of tropospheric velocit
3 2768 001 90970 8
DUDLEY KNOX LIBRARY